

INVESTIGATION OF THE CHANGE IN BMAL1 LEVELS IN RESPONSE TO
MITOCHONDRIAL UNCOUPLING IN HEPG2 CELLS



by
Öykü Boraka

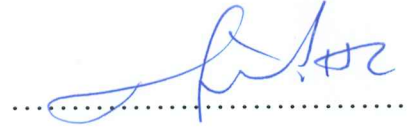
Submitted to Graduate School of Natural and Applied Sciences
in Partial Fulfillment of the Requirements
for the Degree of Master of Science in
Biotechnology

Yeditepe University
2019

INVESTIGATION OF THE CHANGE IN BMAL1 LEVELS IN RESPONSE TO
MITOCHONDRIAL UNCOUPLING IN HEPG2 CELLS

APPROVED BY:

Assist. Prof. Dr. Hüseyin Çimen
(Thesis Supervisor)
(Yeditepe University)



Prof. Dr. Dilek Telci
(Yeditepe University)



Assoc. Prof. Dr. Ceren Çıracı
(Istanbul Technical University)



DATE OF APPROVAL: / / 2019

ACKNOWLEDGEMENTS

I would like to thank to my thesis advisor Assist. Prof. Dr. Hüseyin Çimen for accepting me into the YediPROT team and encouraging my research. I would like to express my sincere gratitude to my dissertation committee members, Prof. Dr. Dilek Telci and Assoc. Prof. Dr. Ceren Çıracı, for reviewing my thesis and their valuable remarks on my work.

I thank to all of my colleagues for their guidance in the laboratory. I would like to express my sincere appreciation to my colleague, İrem Baygutağ, for her precious support throughout my thesis studies.

My special thanks to my beloved grandma, Ayşe Boraka, who had always inspired me with her vibrant, compassionate, and diligent personality. I would like to thank her for raising me, taking care of me and loving me until her last breath. Last but not least, I would like to express my deepest gratitude to my beloved parents Vasfiye Boraka and Zafer Boraka for their invaluable love and support.

ABSTRACT

INVESTIGATION OF THE CHANGES IN BMAL1 EXPRESSION IN RESPONSE TO MITOCHONDRIAL UNCOUPLING IN HEPG2 CELLS

A study in 2016 demonstrated that the rhythmicity in BMAL1 expression was lost and the expression level of BMAL1 significantly decreased in HepG2 cells with depolarized membrane potential. However, the pathway leading to these changes in BMAL1 levels has not been elucidated. In this study, the molecular mechanism behind the changes in BMAL1 levels was investigated. First, the circadian expression of BMAL1 in serum shock-synchronized HepG2 cells was demonstrated by western blot assay. In order to detect the changes in BMAL1 expression more precisely, the timepoint at which BMAL1 levels peak was determined by Cosinor analysis. Mitochondrial membrane potential was measured in trifluoromethoxy carbonylcyanide phenylhydrazone (FCCP)-treated cells to observe if FCCP-induced uncoupling of oxidative phosphorylation led to mitochondrial membrane depolarization. A 79 percent decrease was detected in mitochondrial membrane potential of FCCP-treated cells as a result of confocal laser scanning microscopy analysis of Rhodamine123- and MitoTracker Green FM-stained cells. Next, a specific SIRT inhibitor, EX527 was applied to cells to investigate if there was a link between SIRT1 activity and BMAL1 downregulation in FCCP-treated cells. After confirming SIRT1 inhibition by detecting significant increases in total protein acetylation in EX527-treated cells, BMAL1 expression was investigated by western blot assay. In accordance with the findings in the literature, BMAL1 was downregulated by 63 percent in FCCP-treated cells with respect to control. However, cells which were treated with both FCCP and EX527 were found to have BMAL1 levels similar to the control which indicates SIRT1 inhibition restores BMAL1 downregulation mediated by FCCP. Consequently, SIRT1 activity was considered to be involved in the pathway leading to BMAL1 downregulation in HepG2 cells in response to FCCP-induced mitochondrial membrane depolarization.

ÖZET

HEPG2 HÜCRELERİNDE MİTOKONDRIYAL KENETSİZLENME SONUCUNDA DEĞİŞEN BMAL1 İFADESİNİN ARAŞTIRILMASI

Mitokondriyal membran potansiyelinin bozulmuş olduğu HepG2 hücrelerinde, bir moleküler saat proteini olan BMAL1'in ritmik ifade paterninin bozulduğu ve ifade seviyesinin oldukça düştüğü literatürdeki bir çalışmada ortaya konmuştur; ancak BMAL1 proteininin ifade seviyesindeki bu değişimlerin nasıl gerçekleştiği açığa kavuşturulamamıştır. Bu çalışmada, BMAL1 protein ifadesindeki değişimlerin hangi yolak doğrultusunda gerçekleştiği araştırılmıştır. Öncelikle, serum şoku uygulamasıyla HepG2 hücrelerinin senkronizasyonu sağlanıp BMAL1 proteinin ritmik ifade paterni immunoemdirim tekniği ile elde edilmiştir. BMAL1 proteinin en yüksek ifade seviyesine ulaştığı zaman dilimi ise Cosinor analizi ile, daha sonraki immunoemdirim deneylerinde bu saat örneğini kullanmak üzere, 12. saat olarak tespit edilmiştir. FCCP uygulanan hücrelerde oksidatif fosforilasyonun kenetsizlenmesi sonucunda mitokondriyal membran potansiyelinde bozulma olup olmadığı Rhodamine123 ve MitoTracker Green FM ile boyanan hücrelerin konfokal lazer taramalı mikroskopta incelenmesi ile test edilmiştir. Bunun sonucunda, FCCP uygulanmış hücrelerin mitokondriyal membran potansiyelinde yüzde 79'luk bir düşüş tespit edilmiştir. Daha sonra, BMAL1 ifadesindeki değişimlerin bir deasetilaz olan SIRT1 aracılığıyla gerçekleştiği hipotezine dayanarak, hücrelere bir SIRT1 inhibitörü olan EX527 uygulanmıştır. EX527'nin etkinliğini tespit etmek için toplam protein asetilasyonu seviyesi immunoemdirim tekniğiyle incelenmiştir. Beklendiği gibi, toplam protein asetilasyonunda anlamlı artışlar gözlenmiştir. Son olarak, FCCP, EX527, FCCP ve EX527 uygulanmış örnekler arasında BMAL1 seviyesindeki farklılıklar immunoemdirim tekniğiyle incelenmiştir. Literatürdeki bulgulara uygun olarak, FCCP uygulanmış örneğin BMAL1 seviyesinde kontrole göre yüzde 63'lük bir azalma tespit edilmiştir; ancak FCCP ve EX527'nin birlikte uygulandığı örnekte BMAL1 seviyesinin kontrole yakın olduğu bulunmuştur. Dolayısıyla, SIRT1 enziminin aktivitesinin HepG2 hücrelerinin BMAL1 seviyesinde FCCP uygulaması ile meydana gelen azalmaya yol açan yolak üzerinde etkisi olduğu çıkarımı yapılmıştır.

TABLE OF CONTENTS

ACKNOWLEDGEMENTS.....	iii
ABSTRACT	iv
ÖZET.....	v
LIST OF FIGURES	viii
LIST OF SYMBOLS/ABBREVIATIONS	x
1. INTRODUCTION	1
1.1. CIRCADIAN RHYTHMS	2
1.1.1. Circadian Rhythms in Mammals	2
1.1.2. Circadian Rhythms and Health.....	3
1.1.3. BMAL1	7
1.2. MITOCHONDRIA	8
1.2.1. Mitochondria and Health.....	8
1.2.2. Structure of Mitochondria.....	10
1.2.3. Key Functions of Mitochondria.....	11
1.2.4. Mitochondrial Uncoupling	13
1.2.5. Mitochondria and The Circadian Clock.....	14
1.3. LYSINE ACETYLATION AND SIRTUINS	16
1.3.1. An Overview of Sirtuin Family.....	16
1.3.2. SIRT1 and The Circadian Clock.....	16
1.4. THE AIM OF THE STUDY	18
2. MATERIALS AND METHODS.....	19
2.1. CELL CULTURE	19
2.2. PROTEIN EXTRACTION AND QUANTIFICATION.....	19
2.3. WESTERN BLOT	20
2.4. QUANTITATIVE ANALYSIS OF WESTERN BLOT IMAGES.....	22
2.5. COSINOR ANALYSIS.....	23
2.6. CONFOCAL LASER SCANNING MICROSCOPY.....	23
2.7. QUANTITATIVE ANALYSIS OF CONFOCAL MICROSCOPY IMAGES....	24
2.8. FILTER AIDED SAMPLE PREPARATION.....	25

2.9. MASS SPECTROMETRY-BASED PROTEIN EXPRESSION ANALYSIS	26
2.10. STATISTICAL ANALYSIS	27
3. RESULTS.....	28
3.1. CIRCADIAN EXPRESSION OF BMAL1	28
3.2. LIVE CELL IMAGING BY CONFOCAL LASER SCANNING MICROSCOPY: OPTIMIZATION FOR THREE FLUORESCENT DYES: DAPI, RHODAMINE123, MITOTRACKER GREEN FM.....	30
3.3. MITOCHONDRIAL INNER MEMBRANE POTENTIAL ANALYSIS OF FCCP-TREATED CELLS BY USING RHODAMINE123 AND MITOTRACKER GREEN FM.....	32
3.4. ANALYSIS OF OXIDATIVE PHOSPHORYLATION COMPLEXES IN RESPONSE TO FCCP/EX527/CO- TREATMENT	39
4. DISCUSSION.....	41
5. CONCLUSIONS AND FUTURE PERSPECTIVE	46
REFERENCES	48

LIST OF FIGURES

Figure 1.1. Central clock and peripheral clocks in mammals	3
Figure 1.2. Core circadian clock.....	4
Figure 1.3. Circadian clock-regulated mechanisms and the implications of their disruption on health	5
Figure 1.4. Posttranslational modifications on BMAL1	8
Figure 1.5. Mitochondrial diseases	9
Figure 1.6. Interconnection between TCA cycle, FAO, and OXPHOS pathways	13
Figure 1.7. Mitochondrial and other cellular events controlled by the circadian clock]	15
Figure 1.8. Mechanism of acetylation and deacetylation.....	17
Figure 1.9. Mammalian sirtuin family and their functions.....	17
Figure 3.1. Representative blot of the circadian expression of BMAL1 in HepG2 cells ...	28
Figure 3.2. Rhythmic expression of BMAL1	29
Figure 3.3. The acrophase of circadian BMAL1 expression.....	29
Figure 3.4. DAPI, Rhodamine123 and MitoTracker Green FM stained HepG2 cells.....	31
Figure 3.5. DAPI, Rhodamine123 and MitoTracker Green FM stained HepG2 cells.....	31
Figure 3.6. DAPI, Rhodamine123 and MitoTracker Green FM stained control and FCCP-treated HepG2 cells	32
Figure 3.7. Rhodamine123 stained control and FCCP-treated HepG2 cells.....	33
Figure 3.8. Quantitative Rhodamine123 signal in control and FCCP-treated HepG2 cells	34
Figure 3.9. MitoTracker Gr FM stained control and FCCP-treated HepG2 cells	35
Figure 3.10. Quantitative MitoTracker Green FM signal in control and FCCP-treated HepG2 cells	36
Figure 3.11. Mitochondrial inner membrane potential in control and FCCP-treated HepG2 cells	36

Figure 3.12. Total protein acetylation in FCCP, EX527, or co-treated HepG2 cells at CT12	38
Figure 3.13. Quantitative analysis of total protein acetylation in FCCP, EX527, or co-treated HepG2 cells at CT12	38
Figure 3.14. BMAL1 expression in FCCP, EX527, or co-treated HepG2 cells at CT12 ...	39
Figure 3.15. Quantitative analysis of BMAL1 expression in FCCP, EX527, or co-treated HepG2 cells at CT12.....	39
Figure 3.16. OXPHOS protein expression in FCCP, EX527, or co-treated HepG2 cells at CT12.....	40
Figure 3.17. Quantitative analysis of OXPHOS protein expression in FCCP, EX527, or co-treated HepG2 cells at CT12	40

LIST OF SYMBOLS/ABBREVIATIONS

AD	Alzheimer's disease
AMP	Adenosine monophosphate
AMPK	Adenosine monophosphate-activated protein kinase
ATP	Adenosine triphosphate
BCA	Bicinchoninic assay
BMAL	Brain and muscle ARNT-like
BSA	Bovine serum albumin
CCG	Clock-controlled gene
CK	Creatine kinase
CT	Circadian time
CLOCK	Circadian locomotor output cycles protein kaput
CRY	Cryptochrome
DAPI	4',6-diamidino-2-phenylindole
DMSO	Dimethyl sulfoxide
DNA	Deoxyribonucleic acid
ECL	Enhanced chemiluminescence
ETC	Electron transport chain
FAD	Flavin adenine dinucleotide
FBS	Fetal bovine serum
FCCP	Trifluoromethoxy carbonyl cyanide phenylhydrazine
GTP	Guanosine triphosphate
HD	Huntington's disease
IMM	Inner mitochondrial membrane
IMS	Inter membrane space
K	Lysine
KCN	Potassium cyanide
KO	Knock-out
MMP	Mitochondrial membrane potential
NAD	Nicotinamide adenine dinucleotide

OCR	Oxygen consumption rate
OMM	Outer mitochondrial membrane
OXPPOS	Oxidative phosphorylation
PBS	Phosphate buffer saline
PD	Parkinson's disease
PGC	Peroxisome proliferator-activated receptor gamma coactivator
PER	Period
PMSF	Phenylmethylsulphonyl fluoride
RIPA	Radioimmunoprecipitation assay
ROR	Retinoic acid-related orphan receptor
RORE	Retinoic acid-related orphan receptor responsive element
ROS	Reactive oxygen species
S	Serine
SCN	Suprachiasmatic nucleus
SIRT	Sirtuin
TCA	Tricarboxylic acid
TBS	Tris buffer saline
TBS-T	Tris buffer saline tween
TTFL	Transcription-translation feedback loop

1. INTRODUCTION

The reciprocal relation between the circadian clock and mitochondria has extensively been studied at the genetic level. However, the impact of mitochondrial functionality or mitochondrial redox on the circadian clock has not been investigated thoroughly. In this study, differential regulation of BMAL1 protein was investigated in response to mitochondrial uncoupling in HepG2 cells.

BMAL1 is a master clock protein which functions as a transcription factor in a circadian manner. The word “circadian” is derived from the Latin phrase “circa diem” which is translated to “around a day”, and refers to a 24-hour cycle. Circadian rhythms are defined as biological events which display an endogenous 24-hour rhythmicity independent from physiological temperature, and are entrainable by external factors. Many organisms including bacteria, plants, insects, mammals, and humans possess circadian rhythms [1]. Sleep/wake cycles [2], regulation of body temperature [3], hormone secretions [4] are examples of human circadian rhythms. Mitochondria house many major biochemical pathways in eukaryotic cells. The most important biochemical pathway which mitochondria host is oxidative phosphorylation (OXPHOS) as it is the primary pathway for energy production. OXPHOS is constituted from two processes which are coupled with each other: electron flow through the electron transport chain (ETC) and ATP synthesis driven by chemiosmosis [5]. Coupling of these processes can be disrupted by an electron leak mediated by the uncoupling proteins which are naturally expressed in the cells or by the chemical agents such as trifluoromethoxy carbonyl cyanide phenylhydrazone (FCCP) [6]. Uncoupling of OXPHOS may lead to mitochondrial membrane depolarization based on the intensity of uncoupling.

The circadian rhythm in BMAL1 expression was proven to be lost in HepG2 cells with uncoupled mitochondria. In addition, a sharp decrease BMAL1 levels was observed [7]. The molecular mechanisms behind these changes remain as a mystery. In this project, the loss of rhythmicity and the decrease in BMAL1 levels in cells with uncoupled mitochondria was investigated by employing western blot and confocal microscopy techniques. In a broader perspective, a link between the circadian rhythm and mitochondrial functionality was aimed to be established.

1.1. CIRCADIAN RHYTHMS

1.1.1. Circadian Rhythms in Mammals

Circadian rhythm has two components in mammals; central control in suprachiasmatic nucleus (SCN) in hypothalamus region of the brain, and peripheral clocks in individual cells, tissues, and organs such as endogenous clocks in liver, kidney, pancreas, and lung [8]. The *entrainment* of the central clock is mediated by the light-dark cycles during a 24-hour period [9]. During the day, photic input is received by intrinsically photoreceptive retinal ganglion cells (ipRGCs) to be further conveyed to SCN neurons through the retinohypothalamic tract (RHT) by electrical signals [10]. Light induced activation of SCN neurons triggers neural and hormonal signaling (e.g. glucocorticoid signaling) to further activate other signaling pathways throughout the brain and peripheral organs [11, 12]. Other *Zeitgebers* than the light-dark cycle (a *Zeitgeber* is any external cue which synchronize the internal clock with the external oscillator) which entrain peripheral organs through activation of SCN cells are sleep-wake [13], temperature [14], feeding-fasting rhythms [15]. As a result of this entrainment, circadian rhythms in the brain and body synchronize (Figure 1.1).

Circadian clock is regulated by the master clock proteins at the molecular level; BMAL1, CLOCK, cryptochromes (CRYs), and period proteins (PERs). While BMAL1 and CLOCK constitute the positive arm of the transcription-translation feedback loop (TTFL) and induce the expression of clock-controlled genes (CCGs), CRY and PERs constitute the negative arm of the TTFL and suppress transcriptional activation mediated by BMAL1:CLOCK complex [16]. BMAL1 and CLOCK proteins heterodimerize to function as a transcription factor [17]. BMAL1:CLOCK dimer induces the expression of more than 2000 genes which are referred to as “clock-control genes (CCGs)” [18]. Hence, the molecular clock influences behavior, physiology, and metabolism in a rhythmic manner through its transcriptional activity. All CRYs and PERs are CCGs, thus, the expression of these genes is rhythmically controlled by BMAL1:CLOCK dimer. In return, CRY and PER proteins heterodimerize and act on BMAL1:CLOCK dimer to inhibit its transcriptional activity (20, 21). Thereby, the expression of CCGs including CRYs and PERs are repressed in a negative feedback loop.

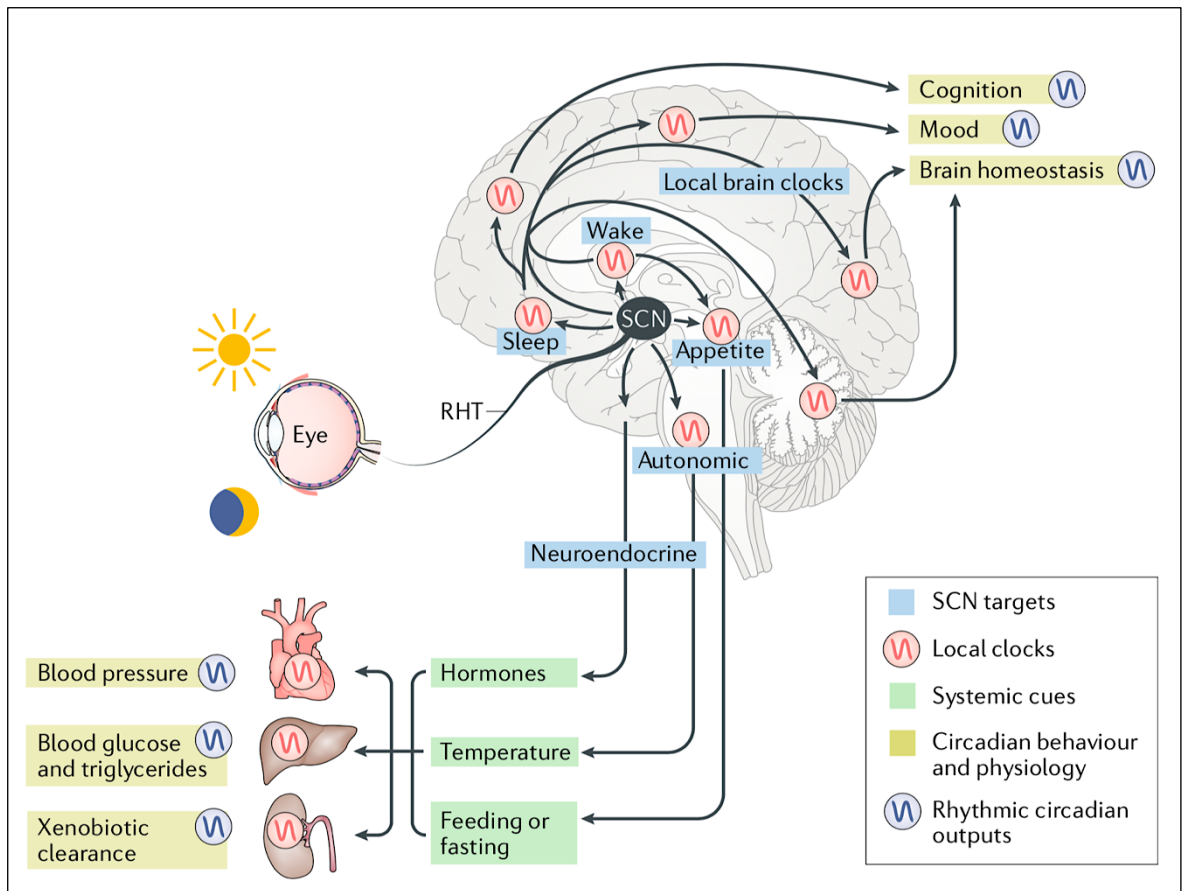


Figure 1.1. Central clock and peripheral clocks in mammals [21]

Other than the master clock proteins, ROR and REV-ERB families control the circadian clock at the cellular level. Both families are nuclear receptor families and compete to bind to the same promoter region of BMAL1 gene which is referred to as ROR responsive elements (ROREs). While RORs activate BMAL1 transcription [22], REV-ERBs inhibit it [23]. Transcription of REV-ERBs are induced by BMAL1:CLOCK [24] (Figure 1.2).

1.1.2. Circadian Rhythms and Health

Since circadian rhythms drive the rhythmic transcription of thousands of genes associated with many key molecular pathways, they not only influence functionality and health of tissues, but they also play a pivotal role in the causation of diseases. Circadian rhythm disruptions have been noted in neurodegenerative disorders, aging, cancer, and metabolic diseases (Figure 1.3).

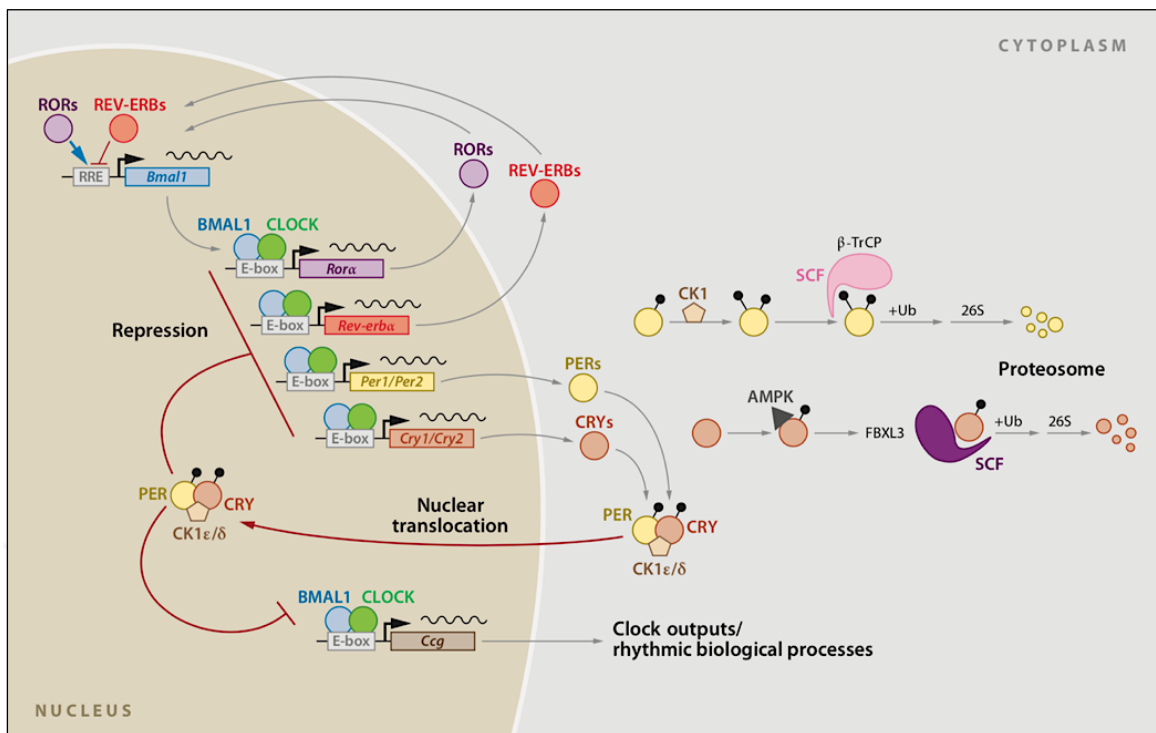


Figure 1.2. Core circadian clock [25]

Patients with neurodegenerative diseases exhibit circadian rhythm disruptions as early symptoms. For instance, Alzheimer's disease (AD) patients display circadian disruptions in their rest-activity [26] cycles while Parkinson's disease (PD) and Huntington's disease (HD) patients have disrupted sleep-wake cycles. It was found that the application of amyloid-beta proteins which are the primary responsible molecules for the development of AD leads to downregulation of BMAL1 in an AD mouse model [27]. In leukocytes derived from PD patients, an abrupt downregulation of *Bmal1* was observed, as well [28]. In a HD mouse model, the rhythmicity of *Bmal1* gene expression was found to be lost [29]. Despite the concrete evidence in the circadian effects of neurodegenerative diseases, the influence of the circadian clock on the causation of diseases has yet to be resolved, and there is only limited research on the issue. Few epidemiologic studies showed that circadian rhythm disruption was associated with an increased risk of dementia. Circadian rhythm disruption was also associated to poor cognitive performance in flight attendants who traveled through multiple time-zones frequently without sparing adequate time to recover [30].

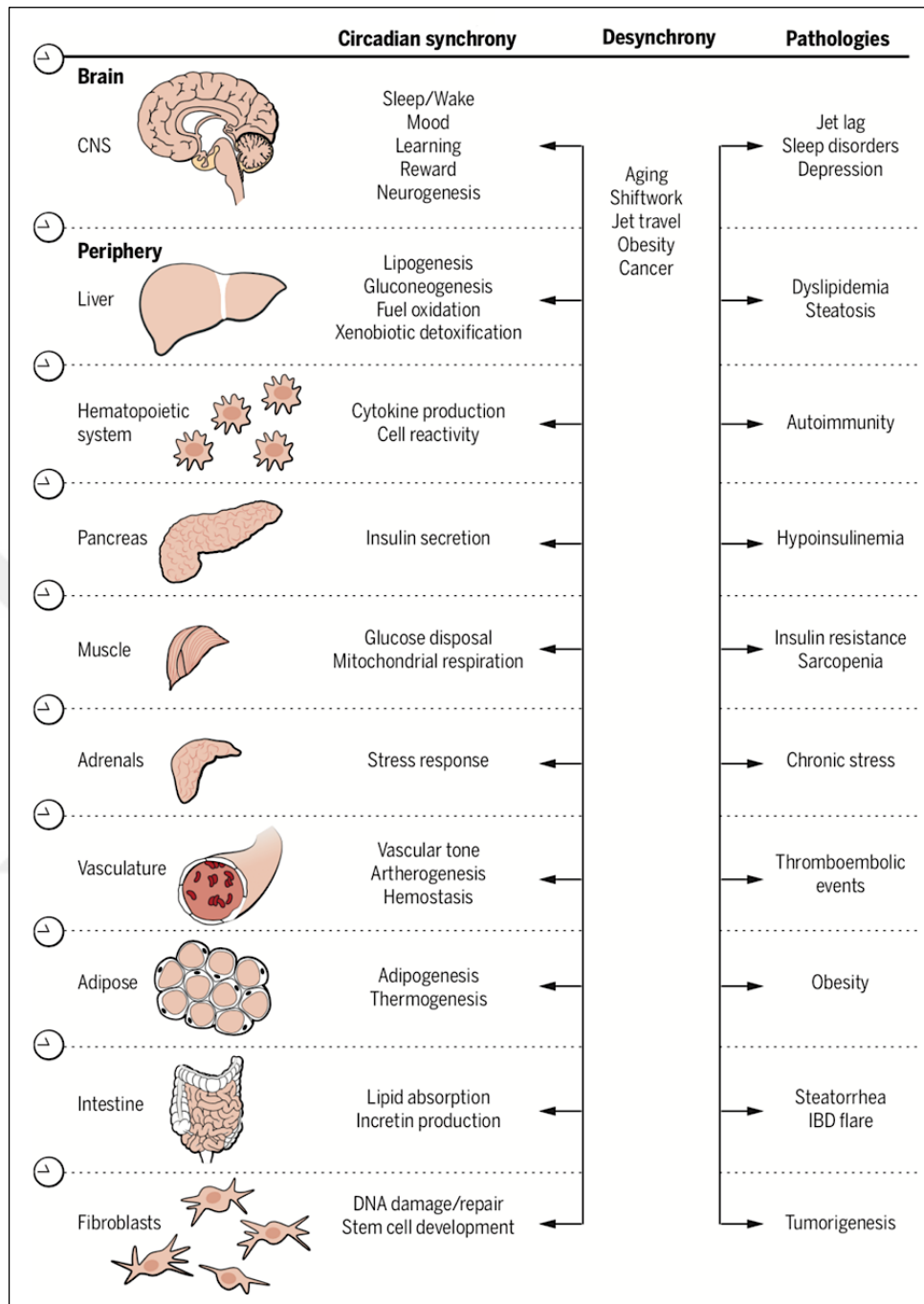


Figure 1.3. Circadian clock-regulated mechanisms and the implications of their disruption on health [31]

In spite of the animal studies and epidemiologic studies, molecular and mechanistic studies in the pathogenesis of neurodegenerative diseases are newly emerging. Manipulations of circadian genes (*per*, *cry*, *reverb*, *bmal1*) in different organisms pointed out that the circadian clock affects lifespan, aging and neurogenesis processes at the molecular level.

For instance, global and brain-specific *bmal1*^{-/-} mice models displayed increased astrogliosis and neurodegeneration, decreased neuroprotection from oxidative damage, and an increased level of brain reactive oxygen species [32]. Furthermore, circadian genes were associated with learning and memory formation [33]. Behavioral studies in rodent models demonstrated that learning and memory formation were reduced in the case of desynchronization of the master clock from external Zeitgebers [34]. In *bmal1* knockout mice models, short term memory formation was disrupted [35]. In another study, *bmal1* knockout mice exhibited a variety of premature aging symptoms which eventually led them to have reduced lifespans [36].

Epidemiologic data shows that the circadian clock genes are dysregulated in many types of human cancers. *Bmal1* gene was found to be dysregulated in breast cancer [37], acute lymphocytic leukemia, acute myeloid leukemia [38], head and neck squamous cell carcinoma [39], malignant pleural mesothelioma [40], diffuse large B-cell lymphoma [41], ovarian cancer [42], prostate cancer [43] patients. *Bmal1* dysregulation contributes to tumorigenesis mainly by affecting target genes involved in oncogenic signaling [44], immune response [45], cell proliferation [46], apoptosis [47], metabolism [48], and DNA repair [49]. Animal studies showed that tumor growth rates were increased in SCN-ablated tumor-bearing mice models compared to tumor-bearing mice models with intact SCN [50]. In vitro studies resulted in either oncogenic or antioncogenic effects in *bmal1*^{-/-} models depending on the cell type used. For example, while serum shock-synchronized skeletal muscle cells and hepatocytes had an upregulated p21 expression which resulted in a decrease in cell proliferation rate [51], primary cells derived from human foreskin fibroblasts became incapable of p53-mediated cell cycle arrest [52].

As circadian clock is tightly associated with metabolism, its disruption may lead to metabolic disorders. For instance, type 2 diabetes patients were found to have circadian rhythm disruptions in glucose metabolism, insulin secretion, and glucose tolerance [53] while type 1 diabetes patients were found to display an altered rhythm of lipolysis [54]. In diabetic animals, it was reported that the expression pattern of circadian clock genes had been changed. In the adipose tissues of obese mice, the rhythmicity in the expression of *bmal1*, *per1/2*, *cry1/2* genes were found to be mildly blunted. However, in the adipose tissues of mice with obesity and diabetes, the rhythmicity in the expression of these genes were blunted severely [55].

Genetically manipulated mice revealed that global knockout of *bmal1* led to a disruption in the oscillation of glucose and triglyceride levels while leading to complete loss of gluconeogenesis. In addition, liver specific *bmal1* knockout mice displayed hypoglycemia during fasting, extreme glucose clearance, and disrupted rhythmicity in the expression of hepatic glucose regulatory genes [56].

1.1.3. BMAL1

BMAL1 protein is encoded by *ARNTL* gene. BMAL1 is a transcriptional activator containing a basic helix-loop-helix (bHLH) domain, two per-arnt-sim (PAS) domains, and a PAS-associated C-terminal (PAC) motif at the C-terminal. BMAL1 is formed of 626 amino acids, having a molecular weight of 68,762 Daltons [57, 58]. Following its translation, BMAL1 is exported to cytosol. As soon as BMAL1 is phosphorylated from its S90 residue by casein kinase 2 α (CK2 α), it heterodimerizes with CLOCK and enters to nucleus [59]. In the nucleus, BMAL1 is phosphorylated from its S17 residue, and CLOCK is phosphorylated from its S427 residue by glycogen synthase kinase 3 beta (GSK-3 β) [60]. Phosphorylated forms of BMAL1 and CLOCK are transcriptionally more active, however, less stable. As BMAL1:CLOCK dimer recruits transcription factors to activate the transcription of clock-controlled genes which is referred to as transactivation, BMAL1 is sumoylated from its K259 residue, then both BMAL1 and CLOCK are ubiquitinated to promote their degradation via proteasomal pathway [61, 62]. Subsequently, another BMAL1:CLOCK dimer recruits on E-box to enhance transcription of CCGs. This cycle of transactivation by degradation is terminated when BMAL1 is acetylated from its K537 residue by CLOCK [63]. CRY1 and PER2 are recruited onto BMAL1:CLOCK dimer so that BMAL1:CLOCK-mediated transcriptional activation is suppressed. CRY1 recruits CK2 β which suppresses CK2 α -mediated phosphorylation of BMAL1. Phosphatases dephosphorylate BMAL1, and SIRT1 deacetylates BMAL1. Finally, CRY1 recruitment onto BMAL1:CLOCK is inhibited, and another cycle of transactivation by degradation starts begins (Figure 1.4). The timing and the order of the posttranslational modifications involved in the molecular clock are crucial for fully functional circadian rhythms.

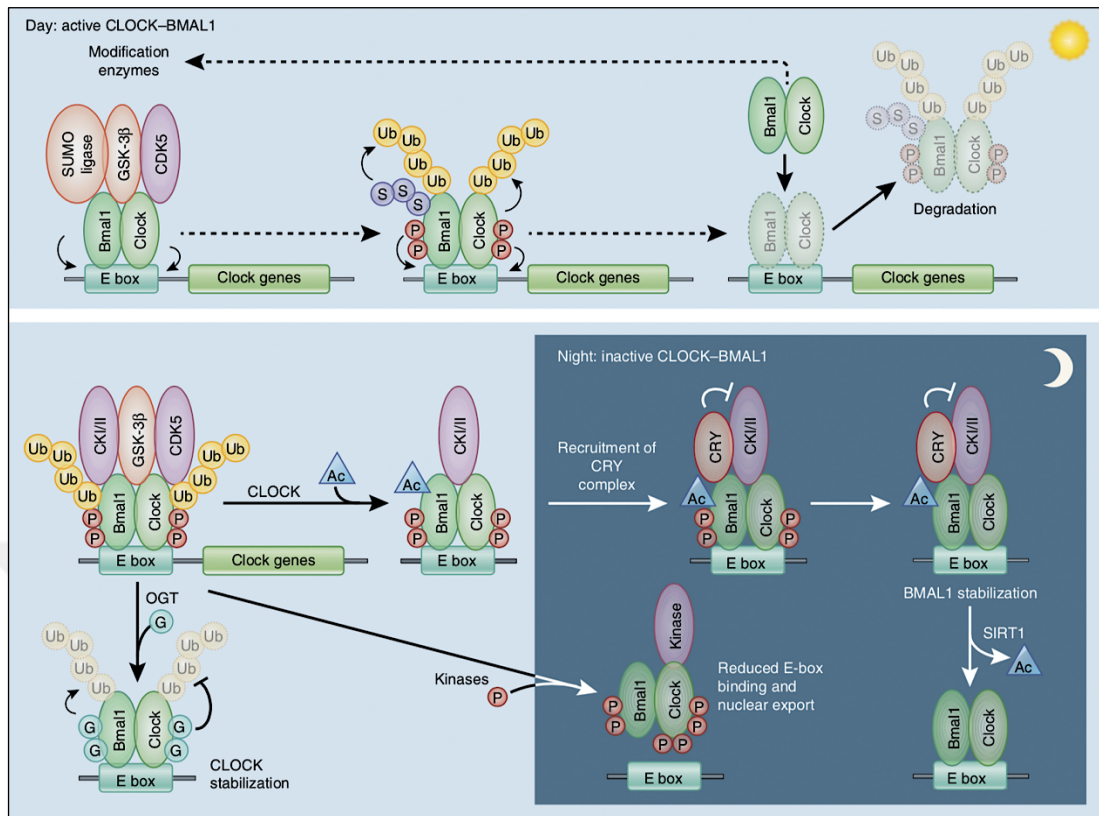


Figure 1.4. Posttranslational modifications on BMAL1 [25]

1.2. MITOCHONDRIA

Mitochondria are the organelles which are mainly in charge of generating energy, and regulating energy metabolism in mammals.

1.2.1. Mitochondria and Health

Since mitochondria are the powerhouses of the cells, they have been associated with a wide spectrum of diseases from mitochondrial diseases to cancer and aging. Mitochondrial diseases are formed as a result of genetic mutations that affect mitochondrial functionality, particularly oxidative phosphorylation. Depending on the affected tissue or organ, mitochondrial dysfunction can lead to a variety of health conditions from neurological conditions such as hearing loss [64], Parkinson's disease [65], and myopathy [66, 67] to

non-neurological disorders such as liver failure [68], diabetes mellitus [69], and bone marrow failure [70] (Figure 1.5).

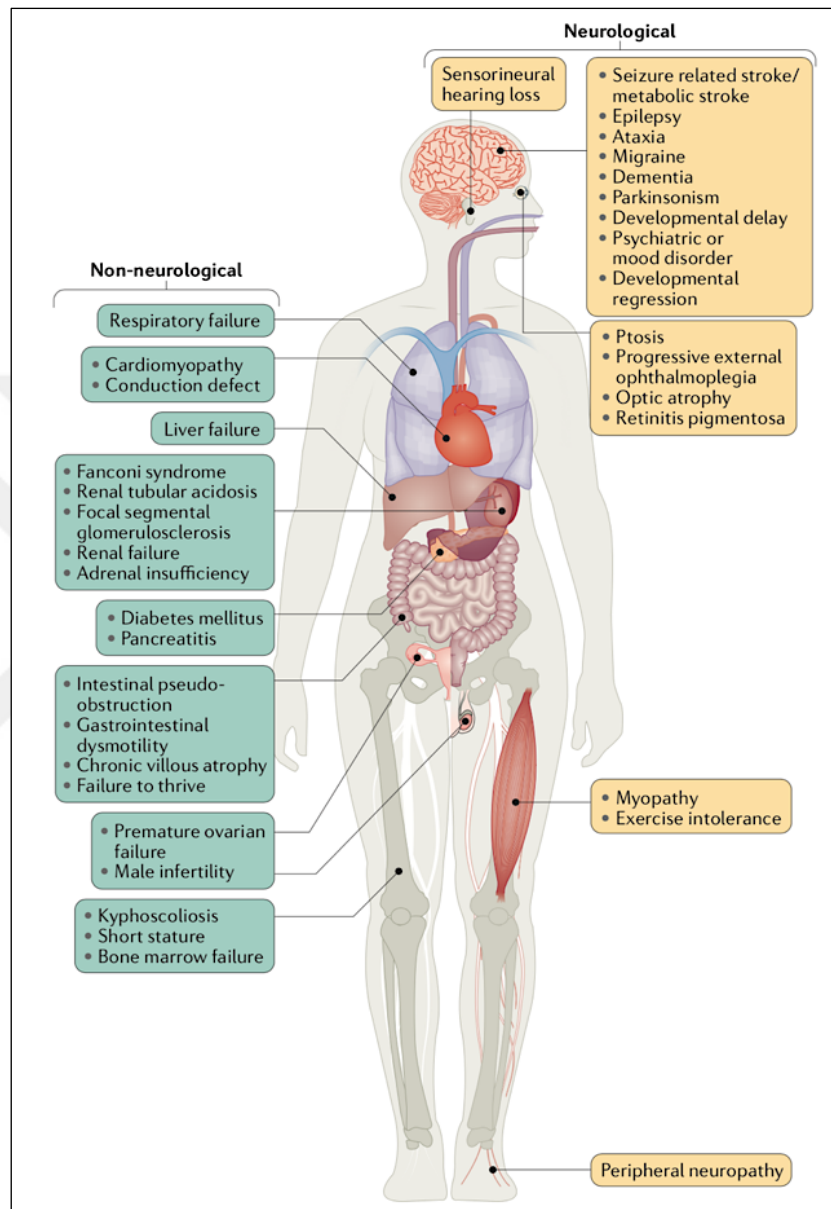


Figure 1.5. Mitochondrial diseases [71]

The role of mitochondria in cancer have extensively been investigated. Mitochondria directly influence tumorigenesis since they are at the center of the intrinsic apoptosis pathway. When intracellular signals such as DNA damage or oxidative stress are sensed, proapoptotic factors (BAK, BAX) are activated, and pores are formed in the outer mitochondrial membrane. As a result, cytochrome *c* molecules are released out of the

mitochondria, into the cytosol, to further activate caspase-mediated apoptosis pathway. The binding of proapoptotic factors to mitochondria can be inhibited by antiapoptotic factors (BCL2) for the survival of the cells [72].

In addition to the intracellular signals, mitochondrial reactive oxygen species (ROS) can trigger cytochrome *c* release and activate the caspase-dependent apoptosis pathway [73]. In order to sustain a low ROS level, mitochondria must have an intact membrane potential (MMP) which can couple the electron transport with OXPHOS so that only a few electrons would leak to form ROS [74]. On the contrary, growing evidence demonstrate that increased levels of ROS mediates cell survival [75]. Other mitochondrial events that have been linked to cancer are mitochondrial biogenesis, mitophagy, fission and fusion. PGC1- α is a nuclear transcription factor that drives mitochondrial biogenesis. Besides the low levels of PGC1- α in renal cell carcinoma, overexpression of PGC1- α acts as a tumor suppressor in some cancer types. On the other hand, growing evidence show that PGC1- α can also bear metastatic potential [76]. Mitophagy which is mainly controlled by PINK1/PARKIN pathway, can also be protumorigenic or antitumorigenic depending on the cancer stage [77]. Mitochondrial dynamics are of crucial importance as they determine the morphology of mitochondria, thus, the energetics and functionality. Hence, the balance between fission and fusion processes must be maintained to facilitate mitochondrial functionality. Shifting the balance towards fission leads to an abundance of fragmented mitochondria which are less functional in the means of oxidative phosphorylation. As a result, an unbalanced mitochondrial dynamics can lead to an increment in ROS levels, and apoptosis [78].

Mitochondria have been also associated with aging. While healthy mitochondria modulate a successful aging process, damaged mitochondria contribute to pathophysiology of aging related diseases. The delicate balance between mitochondrial biogenesis and turnover, mitochondrial dynamics, the efficiency of oxidative phosphorylation, an intact MMP, and low levels of ROS formation are key to healthy aging [79].

1.2.2. Structure of Mitochondria

Mitochondrial membrane is constituted of an outer mitochondrial membrane (OMM) and an inner mitochondrial membrane (IMM). Outer membrane contains porins which permits

the diffusion of small molecules (<50 kDa), such as ions. TOM and SAM complexes which function in protein import to mitochondria and voltage-dependent anion channel (VDAC) which function in metabolite transport reside at OMM. On the other hand, inner membrane does not have a porous structure, therefore, is highly impermeable except for CO₂, O₂ and H₂O. OXPHOS complexes (CI-V), fusion and fission proteins (mitofusins, OPA1 and DNMI, DRP1, respectively), protein import machinery (TIM complexes, ion transporters (permeability transition pore, adenine nucleotide transporter, pyruvate carriers etc.), uncoupling proteins, proteins involved in heme synthesis are embedded into IMM. IMM is extensively folded towards the mitochondrial matrix. These folds are referred to as cristae and they are the main sites where OXPHOS occur. Finally, mitochondrial ribosomes, mtDNA, and the proteins involved in various biochemical pathways such as tricarboxylic acid (TCA) cycle, fatty acid oxidation, amino acid metabolism, urea cycle, cardiolipin synthesis, biosynthesis of Fe-S clusters, and antioxidant defense are contained in the mitochondrial matrix [80].

1.2.3. Key Functions of Mitochondria

The major function of mitochondria is to supply energy to the cells. The main pathway for energy production is oxidative phosphorylation, in other words, aerobic respiration. Other than OXPHOS, TCA cycle is crucial for energy production as it provides redox equivalents which are required for electron and H⁺ transport to IMM and intermembrane space (IMS), respectively. After pyruvate is imported via the mitochondrial pyruvate carrier (MPC), it is either incorporated into gluconeogenesis or TCA cycle. In the latter, pyruvate is oxidized into acetyl CoA by pyruvate dehydrogenase as a molecule of NADH and CO₂ are generated. The two carbons of acetyl CoA are incorporated to the four-carbon compound oxaloacetate by citrate synthase to form a six-carbon molecule, citrate which is a type of tricarboxylic acid. After the conversion of citrate to isocitrate by aconitase, two subsequent oxidation reactions take place. Along with the formation of NADH and CO₂ at each reaction, α -ketoglutarate and succinyl CoA are formed, respectively. The four-carbon succinyl CoA is further converted to succinate coupled with substrate-level phosphorylation which generates one molecule of GTP. In another redox reaction, fumarate and FADH₂ are formed by succinate dehydrogenase. In the meantime, ubiquinone (Q) is reduced to ubiquinol (QH₂). Malate is formed after addition of one H₂O

molecule. Finally, malate is oxidized back to oxaloacetate and NADH is generated. As a result of one TCA cycle, two molecules of CO₂, a molecule of GTP, three molecules of NADH, and a molecule of FADH₂ are formed [81].

Another mitochondrial key pathway regarding energy metabolism is beta oxidation of fatty acids. Fatty acyl CoA molecules react with carnitine molecules to generate fatty acyl carnitine. Fatty acyl carnitines are transported into mitochondria via carnitine shuttle which is composed of carnitine palmitoyltransferase-1 (CPT1), carnitine acylcarnitine translocase (CACT), carnitine palmitoyltransferase-2 (CPT2) proteins. Fatty acyl carnitine molecules are converted back to acyl CoA molecules by CPT2 and incorporated into beta oxidation pathway where they are completely oxidized down to acetyl CoA molecules to be used in TCA cycle. In addition, redox equivalents NADH and FADH₂ which are consumed by respiratory complexes for energy production via OXPHOS are generated. The enzymes involved in beta oxidation pathway are acyl CoA dehydrogenase, enoyl-CoA hydratase, 3-L-hydroxyl-CoA dehydrogenase, and β -ketothiolase, respectively [82].

OXPHOS is the main pathway for energy production in eukaryotes. In OXPHOS, the energy stored in redox equivalents NADH and FADH₂ are used to drive ATP synthesis. Thus, OXPHOS can be divided into two parts; electron transport to the final electron acceptor in the ETC, cytochrome *c* oxidase (complex IV), and ATP synthesis driven by ATP synthase (complex V). These two processes are coupled to each other with a mechanism referred to as chemiosmotic coupling. According to the chemiosmotic theory, the energy required to synthesize ATP from ADP is derived from the protonmotive force which has two components; MMP (electrical contribution) and the difference in H⁺ ion concentration between the MMP and the matrix (chemical contribution) as depicted below.

$$\Delta p(mV) = \Delta\psi - 59\Delta pH \quad (1.1)$$

The pH and voltage differences between IMS and matrix favor the movement of ions into the matrix down their electrochemical gradient. The electrons which are carried by NADH and FADH₂ are transferred to Fe-S clusters in NADH dehydrogenase (complex I) and succinate dehydrogenase (complex II), respectively. In the meantime, protons derived from redox equivalents are pumped into IMS. Thus, an electrochemical gradient is formed.

Electrons are sequentially transferred to ubiquinone (coenzyme Q), coenzyme Q:cytochrome *c* oxidoreductase (complex III), cytochrome *c*, and to cytochrome *c* oxidase (complex IV) (Figure 1.6).

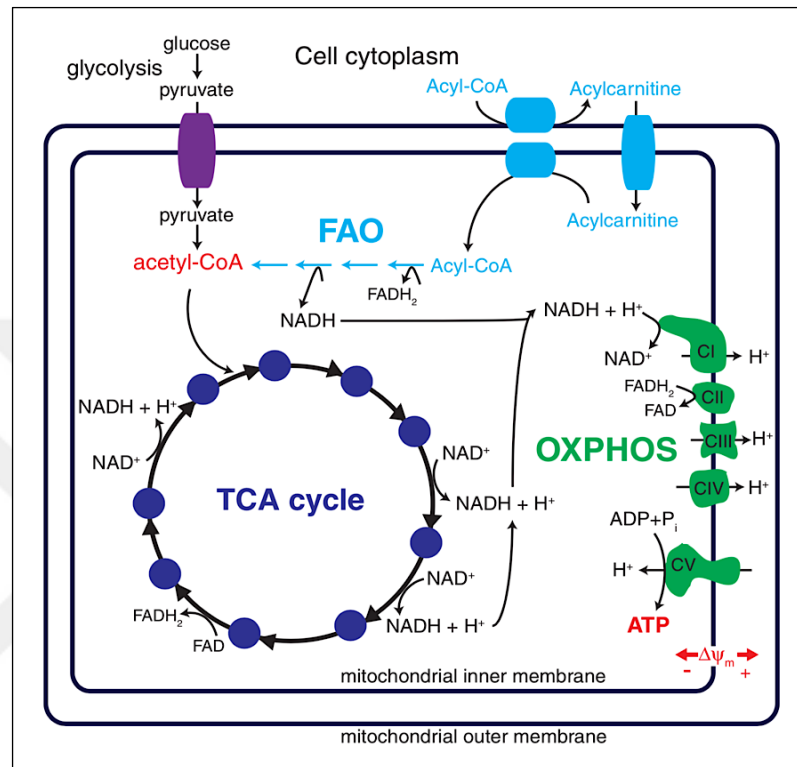


Figure 1.6. Interconnection between TCA cycle, FAO, and OXPHOS pathways [83]

Finally, complex IV produces H_2O by using the electrons diffused back into the matrix down their electrical gradient. Coupled with H_2O formation, protons are diffused back to the matrix down their concentration gradient through F_0F_1 ATP synthase. By using the electrochemical gradient and the free energy released from H_2O formation, ATP synthase catalyzes ATP synthesis reaction forward [25].

1.2.4. Mitochondrial Uncoupling

The chemiosmotic coupling that drives oxidative phosphorylation can be disrupted by protonophores such as FCCP or physiologic uncoupling mediated by uncoupling proteins. Both processes involve the transport of H^+ from the IMS into the matrix, therefore, create

an alternative route to the diffusion of H^+ through ATP synthase which facilitates ATP synthesis through this process [6]. Uncoupling of OXPHOS leads to a decline in ATP levels, and an incline in thermogenesis because the energy preserved in the proton gradient is dissipated as heat. In addition, respiration, therefore, NADH oxidation is induced to restore the decreased proton concentration in the IMS [84]. The decrease in the efficiency of OXPHOS is highly dependent on the severity of uncoupling. While severe uncoupling results in mitochondrial dysfunction due to mitochondrial membrane depolarization, mild uncoupling does not necessarily disrupt the MMP [85]. In fact, mild uncoupling has been found to have cardioprotective [86] and antiaging effects [87] since it reduces ROS formation and increases metabolic rate [88].

1.2.5. Mitochondria and The Circadian Clock

Organelles exhibit diurnal rhythmicity in their functions. Mitochondria, as well as other organelles, functions rhythmically since the molecular clock temporally controls mitochondrial events through its transcriptional activities. One example of the mitochondrial impact of the circadian clock would be the rhythmic generation of NAD^+ as NAD^+ is a vital metabolite which is involved in TCA cycle, and a cofactor for the catalytic activity of both sirtuins and poly-ADP-ribosyl polymerases. BMAL1:CLOCK dimer modulates the rhythmic expression of nicotinamide phosphoribosyltransferase (NAMPT) which takes part in the biosynthetic pathway of NAD^+ [89]. For example, the activity of complex I (NADH dehydrogenase) is rhythmically controlled, as well. Deacetylation of CI is rhythmic due to rhythmic sirtuin activity mediated by the rhythmic expression of NAD^+ (Figure 1.7) [90]. Bmal1 knockout mice exhibited impaired OXPHOS, and downregulated SIRT3 activity in accordance with the circadian cycle of NAD^+ [91]. The catalytic contribution of dynamin-related protein 1 (DRP1) which is a mitochondrial fission regulating protein is controlled by the circadian clock, as well. DRP1 is rhythmically phosphorylated, and when it is phosphorylated, the balance between fusion and fission shifts toward fusion. Hence, mitochondria become more tubular rather than fragmented, and the rate of oxidative phosphorylation increases [92]. The expression levels of succinate dehydrogenase 1, a complex II subunit, in both gene and protein levels are rhythmic in liver [93]. Heart-specific bmal1 knockout mice exhibited a substantial downregulation in the transcription of TCA cycle, FAO, and OXPHOS genes [94].

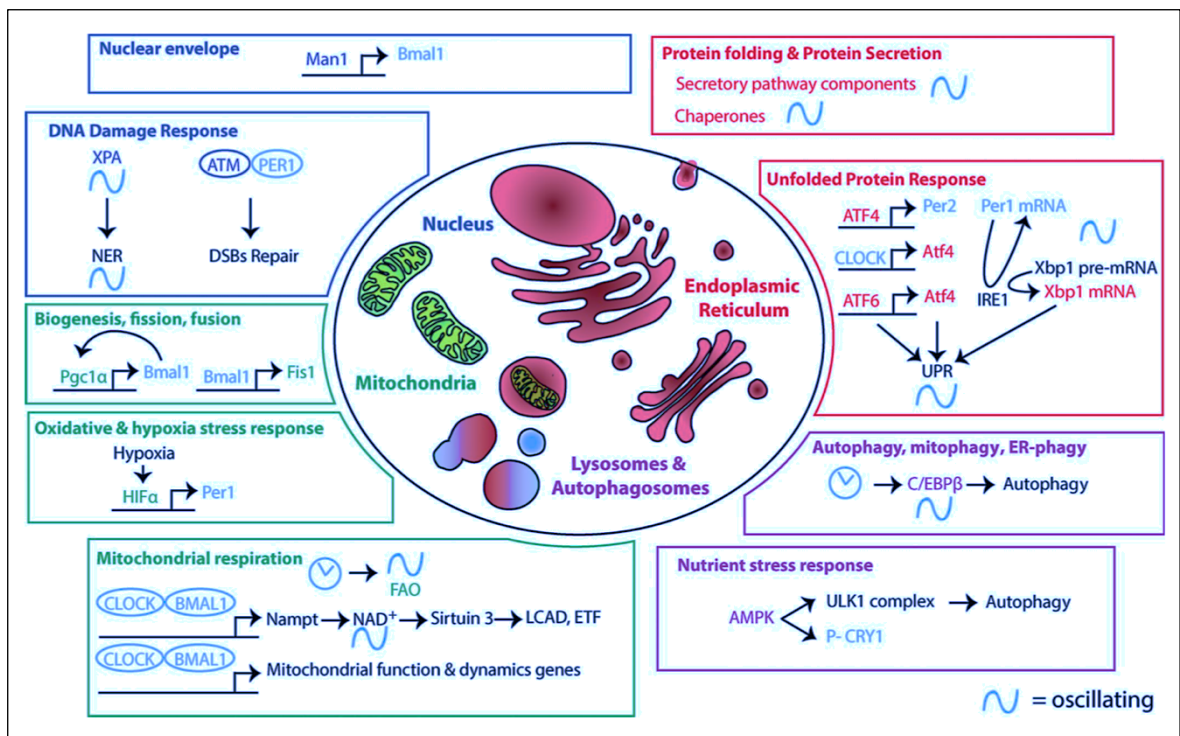


Figure 1.7. Mitochondrial and other cellular events controlled by the circadian clock [95]

The levels of fatty acids, triacylglycerides, glycerophospholipids, sterol lipids, and sphingolipids are found to be rhythmic in blood plasma [96]. The rhythmicity in glucose and triglyceride levels in blood plasma are lost in both BMAL1 KO mice and in mice with mutated CLOCK which indicates the circadian clock controls glucose homeostasis [96, 97]. PGC1- α is rhythmically expressed in HepG2 cells [90] and in the livers of mice [99]. In cardiac tissues of BMAL1 KO mice, *pgc1- α* is downregulated. In these tissues, the expression and activity of ETC components are also found to be downregulated [94]. In the muscles of BMAL1 KO mice, mitochondrial volume and OCR are decreased [100]. Additionally, OCR is decreased in the livers of liver-specific BMAL1 KO mice [101]. These data suggest that aerobic respiration is rhythmically regulated.

Transcriptional coactivator of mitochondrial energy metabolism, PGC1- α , coactivates the expression of *bmal1* through binding to its promoter region so that it alters the local chromatin to an active conformation, and stimulates ROR α -activated *bmal1* expression [99]. In addition, it was found that BMAL1 levels significantly decreased and lost its rhythmicity in HepG2 cells which had EtBr-, FCCP-, or KCN- induced mitochondrial dysfunction [102].

1.3. LYSINE ACETYLATION AND SIRTUINS

1.3.1. An Overview of Sirtuin Family

Sirtuins are enzymes which are primarily responsible for catalyzing protein deacetylation by using NAD^+ as cofactors. They catalyze the deacetylation reaction where they remove the acetyl (CH_3CO) group from their targets as they convert NAD^+ into nicotinamide (NAM) and 2'-O-acetyl-ADP-ribose (Figure 1.8). Since the presence of an acetyl group on proteins affects their activities, sirtuins are capable of either activating or inactivating their target proteins depending on local NAD^+ concentration [103]. Seven sirtuin isoforms are present in mammalian cells. SIRT1 and SIRT2 are placed in nucleus and cytoplasm. SIRT4 and SIRT5 are placed in mitochondria, only. SIRT6 and SIRT7 are placed in nucleus, only. SIRT3 is localized in mitochondria and nucleus. In addition to their deacetylation activity, sirtuins can catalyze other enzymatic reactions depending on the isoform. For example, SIRT5 can catalyze desuccinylation and demalonylation reactions, as well as deacetylation (Figure 1.9).

1.3.2. SIRT1 and The Circadian Clock

SIRT1 is found to deacetylate both histones and BMAL1 which are previously acetylated by CLOCK [104]. A further study demonstrated that SIRT1 mediated BMAL1:CLOCK transcriptional activation led to rhythmic expression of NAMPT, thus, rhythmic production of its own cofactor, NAD^+ [105]. Nevertheless, deacetylation of BMAL1 mediated by SIRT1 remains as a controversial finding as SIRT1 is also found to deacetylate PER2 [106]. The controversy arises from the fact that BMAL1 acetylation increases the amplitude of the molecular clock while PER2 acetylation decreases the amplitude of the molecular clock [107]. Moreover, SIRT1 is found to downregulate per2 expression by deacetylating the local histone on per2 promoter [108].

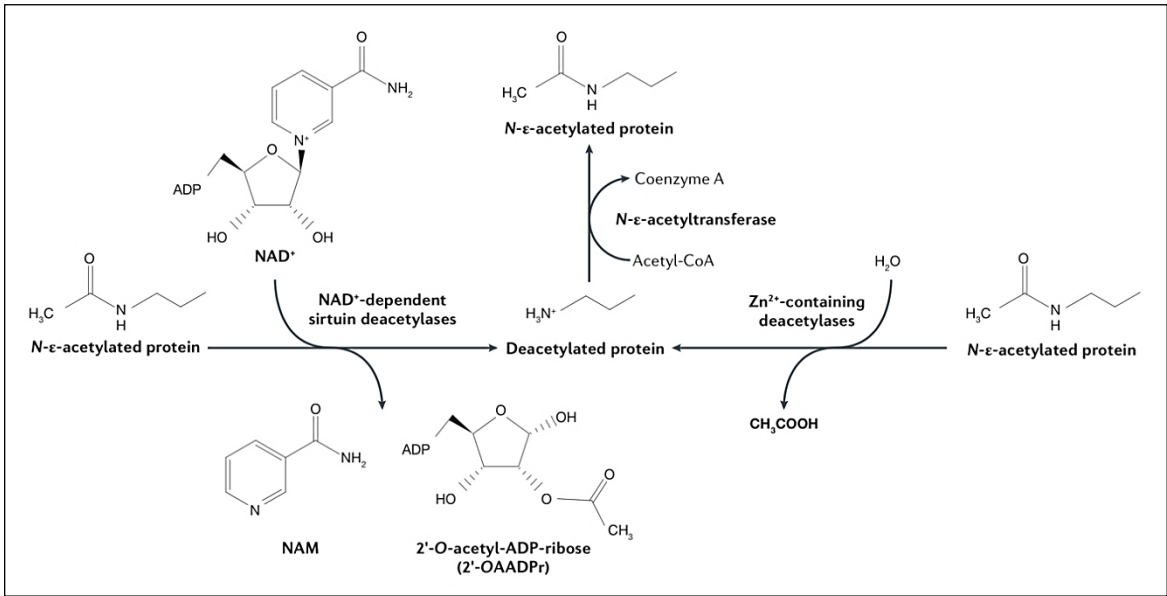


Figure 1.8. Mechanism of acetylation and deacetylation [109]

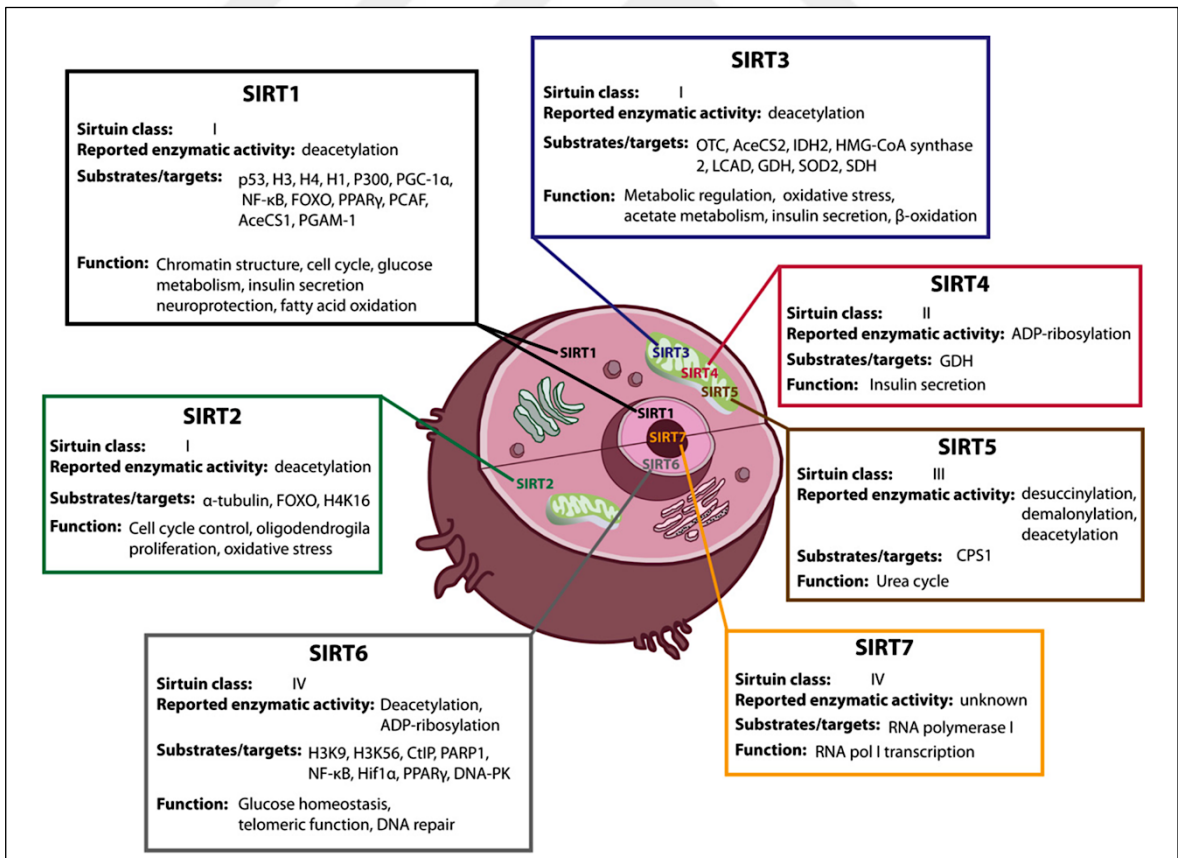


Figure 1.9. Mammalian sirtuin family and their functions [110]

1.4. THE AIM OF THE STUDY

The rhythmic expression of BMAL1 was found to be lost in HepG2 cells with EtBr-, FCCP- or KCN- induced mitochondrial dysfunction [7]. These chemicals were used to deplete cells from mtDNA, uncouple oxidative phosphorylation, or inhibit respiratory complex IV, respectively. The loss of rhythmicity in BMAL1 expression is accompanied by its downregulation in all conditions. The molecular mechanism behind the changes in BMAL1 expression pattern in these cells has not been elucidated yet. The aim of this study is to enlighten the molecular mechanism behind the downregulation and the loss of rhythmicity in BMAL1 expression in response to FCCP-induced mitochondrial uncoupling in HepG2 cells. In order to achieve that aim, immunoblotting and mass spectrometry-based protein expression analysis were performed for HepG2 cells treated with EX527, which inhibits SIRT1. In a broader perspective, a novel link between mitochondrial functionality and the circadian clock is aimed to be established in redox-mediated and sirtuin-dependent contexts.

2. MATERIALS AND METHODS

2.1. CELL CULTURE

HepG2 (*Homo sapiens*, liver, hepatocellular carcinoma, ATCC® HB-8065™) cells were grown in DMEM Low Glucose Media (Gibco™ DMEM, low glucose, pyruvate #31885023) supplemented with 10 percent fetal bovine serum (FBS) (Gibco™ Fetal Bovine Serum, qualified, heat inactivated, United States #16140-063) and 1 percent Pen-Strep (Gibco™ Penicillin-Streptomycin (5,000 U/mL #15070-063). 3×10^6 HepG2 cells were seeded into T25 flasks and incubated overnight for complete attachment. On the day of the experiment, the circadian rhythms of the cells were synchronized by serum shock which involves incubating the cells with 50 percent FBS-containing media for two hours. After the point when the media was switched to serum-free media which had been denoted as the 0th hour sample, synchronized cells were collected every three hours for a complete 24-hour period (3rd, 6th, 9th, 12th, 15th, 18th, 21st, 24th hour samples). For FCCP (Abcam, ab120081) treatment, the cells were treated with 0.6 μ M FCCP during serum shock. For EX527 (Sigma-Aldrich, E7034) treatment, cells were treated with 50 mM EX527 for 16 hours before serum shock, during serum shock, and after serum shock until cells were collected at the 12th hour.

FCCP stock (20 mM) was prepared by dissolving 10.16 mg of FCCP in 2 ml of dimethyl sulfoxide (DMSO). It was diluted 1:20 fold in DMSO to a final concentration of 1 mM. 2.4 μ l of 1 mM FCCP was applied to cells in T25 flasks in a final volume of 4 ml of media. EX527 (10 mM) stock was prepared by dissolving 5 mg of EX527 in 2 ml of DMSO. 20 μ l of 10 mM EX527 was applied to cells in T25 flasks in a final volume of 4 ml of media. All the materials were equilibrated to room temperature before using.

2.2. PROTEIN EXTRACTION AND QUANTIFICATION

Cell pellets obtained from T25 flasks were dissolved with 500 μ l of RIPA lysis buffer (Santa Cruz Biotechnologies, sc-24948) supplemented with 1 percent protease inhibitor cocktail, 1 percent sodium orthovanadate, and 1 percent deacetylase inhibitor cocktail.

After 30 minutes of incubation on ice, cell suspensions were centrifuged at 14,000 g for 15 minutes at 4°C. The supernatants were kept as protein samples.

The bicinchoninic acid (BCA) assay (Thermo Scientific™ Pierce™ BCA Protein Assay Kit, #23225) was performed to determine the protein concentrations in the samples. Samples were diluted 1:5. BCA reagent was prepared by mixing reagent A and reagent B with a 50:1 ratio. 5 µl of each diluted sample were added to a 96-well plate. On top of each sample, 100 µl of BCA reagent was added. The plate was covered with folio and the reaction was let to take place at 37°C for 30 minutes. After cooling down, absorbances of the purple colored-products were measured at 562 nm. Protein samples were stored at -20°C in aliquots after the addition of 1 percent phenylmethylsulphonyl fluoride (PMSF) to each tube.

2.3. WESTERN BLOT

Sample containing 20 µg of protein was loaded to a 10 percent acrylamide gel. Gel was run at 90 V for 20 minutes and 120 V for 90 minutes. After the run was finished, the gels were equilibrated in Bjerrum-Schafer Nielsen transfer buffer (pH = 9.2) with 10 percent methanol and 0.05 percent SDS for 15 minutes. Meanwhile, four filter papers (each 0.84 mm thick) and a methanol-activated PVDF membrane were equilibrated in transfer buffer for 15 minutes. The transfer sandwich was then stacked in the following order on the anode platform of the Thermo G2 Fast Blotter transfer device: two filter papers, membrane, gel, two filter papers. Any bubble left in the sandwich was squeezed out with the help of a roller. After placing the cathode platform and locking the transfer device, transfer was let to take place for 24 minutes at constant current (0.3-0.4 A). After transferring of proteins from the gel to the membrane, the membrane was blocked with 5 percent dry milk powder solution in tris-buffered saline supplemented with 0.1 percent Tween-20 (TBS-T) for an hour at room temperature on a gyro-rocker. Membrane was rinsed with TBS-T briefly for three times. Later, the membrane was incubated with 1:1000 diluted anti-BMAL1 (Cell Signaling Technology, BMAL1 (D2L7G) Rabbit mAb #14020) antibody solution prepared in 5 percent dry milk powder solution for 16 hours at 4°C. Next day, the membrane was washed thrice with TBS-T for 5 minutes.

The membrane was incubated with 1:2000 diluted secondary antibody (Sigma-Aldrich, Anti-Rabbit IgG-Peroxidase antibody produced in goat, A6154) 1 hour at RT.

After washing thrice with TBS-T for 5 minutes, the membrane was incubated with 1.5 ml of ECL substrate mix (Bio-Rad, Clarity™ Western ECL Substrate, #1705061) prepared in 1:1 ratio for 5 minutes. Chemiluminescence signals were detected from protein bands with the use of Bio-Rad ImageLab Version 6.0.0 and Bio-Rad ChemiDoc™ XRS+ system. Signals were quantified by using ImageLab and normalized to their respective controls.

To detect total protein acetylation, wet transfer method was employed after SDS-PAGE. Towbin transfer buffer with 20 percent methanol was used to equilibrate the transfer materials including the fiber pads, and for the transfer. The transfer sandwich was stacked in the following order on the anode side of the gel holder cassette of the Bio-Rad Mini Trans-Blot Electrophoretic Transfer Cell system: fiber pad, two filter papers, membrane, gel, two filter papers, fiber pad. After closing the gel holder cassette firmly, it was placed into the electrode module. The electrode module and a blue cooling unit were placed into the buffer tank. After the addition of ice-cold transfer buffer, the tank was embedded into a container filled with ice. Transfer was let to take place for an hour at constant current (0.35 A). After transferring of proteins from the gel to the membrane, the membrane was blocked with 5 percent bovine serum albumin (BSA) solution in TBS-T for an hour at room temperature on a gyro-rocker. Membrane was rinsed with TBS-T briefly for three times., The membrane was incubated with 1:1000 diluted anti-acetylated-lysine antibody (Cell Signaling Technology, Acetylated-Lysine Mouse mAb (Ac-K-103) #9681) solution prepared in 2.5 percent BSA solution for 16 hours at 4°C. Next day, the membrane was washed thrice with TBS-T for 5 minutes. The membrane was incubated with 1:5000 diluted secondary antibody (Sigma-Aldrich, Anti-Mouse IgG-Peroxidase antibody produced in rabbit, A9044) 1 hour at RT. After washing thrice with TBS-T for 5 minutes, 1 ml of ECL substrate mix which was prepared in 1:1 ratio by using 0.1 ml of each reagent and 0.8 ml of TBS, was poured on top of the membrane. Chemiluminescence signals were detected from protein bands with the use of ImageLab software and ChemiDoc XRS+ system. Signals were quantified by using ImageLab and normalized to their respective controls.

To detect each subunit of the oxidative phosphorylation complexes, the protocol above had been used except that the membrane was blocked with 5 percent dry milk powder solution, and the total anti-OXPHOS rodent antibody cocktail (Abcam, ab110413) was diluted 1:5000 fold.

After obtaining the images, the membranes were washed five times with TBS-T for 10 minutes. The membranes were then incubated 1:5000 diluted anti- β -ACTIN (Santa Cruz Biotechnologies, β -Actin(C4) mouse mAb, sc-47778) antibody solution for 16 hours at 4°C. Next day, the membrane was washed thrice with TBS-T for 5 minutes. The membrane was incubated with 1:5000 diluted secondary antibody (anti-mouse) 1 hour at RT. After washing thrice with TBS-T for 5 minutes, 1 ml of ECL substrate mix which was prepared in 1:1 ratio by using 0.1 ml of each reagent and 0.8 ml of TBS, was poured on top of the membrane. Chemiluminescence signals were detected from protein bands with the use of Image Lab software and ChemiDoc XRS+ system.

2.4. QUANTITATIVE ANALYSIS OF WESTERN BLOT IMAGES

Quantitation of the blot images were performed by using Image Lab software. The raw files in the .scn format were opened in the software. In each image, the lanes were selected, adjusted, and then the bands were added and adjusted through the “Lane and Bands” tab at the Analysis Tool Box. Afterwards, lane profiles were checked and the borders of the bands were corrected through the “Lane Profile” tab. The background signal was totally subtracted for the quantitation of BMAL1 and β -ACTIN signals, however, kept for the quantitation of total protein acetylation signals. Quantitative data of each band in the image was obtained from the “Lane Statistics” tab at the Analysis Table. “Adjusted total band volume (Int)” values of each band were transferred to a Microsoft Excel file. For each experiment, the signal of the protein of interest was divided to the signal of the housekeeping protein which had been β -ACTIN for all experiments by using Microsoft Excel 16.9.9. The normalized values of all samples (control, FCCP-treated, EX527-treated, and co-treated) obtained from three experiments were further divided to the average of normalized control signals, and multiplied by 100. The averages and standard deviations of the normalized values were finally calculated, and used to construct a bar graph.

2.5. COSINOR ANALYSIS

Cosinor analysis of the circadian expression of BMAL1 was done by using “psych” package in R 3.5.0.

After the installation of R, “psych” package was downloaded and installed through the Package Installer embedded in R. A code which contained the time intervals and their respective normalized signals was used to obtain the graph of the rhythmic BMAL1 expression over a 24-hour period (Algorithm 2.1).

Algorithm 2.1. Cosinor analysis algorithm

```
library (psych)
Time=c(0,3,6,9,12,15,18,21,24)
Densitometry=c(100,99,218,319,306,332,161,83,142)
cosinor(Time,Densitometry)
timeTemp <- data.frame(Time,Densitometry)
cosinor.plot("Time","Densitometry",data=timeTemp)
```

2.6. CONFOCAL LASER SCANNING MICROSCOPY

HepG2 cells (10^6) were seeded to cover slips on a six-well plate prior the day of the experiment. After complete attachment, cells were incubated with 5 $\mu\text{g/ml}$ DAPI (Sigma-Aldrich, D9542) in incomplete media for 2 hours in the incubator. After 3 brief washes with 1x dPBS, cells were incubated with 5 $\mu\text{g/ml}$ Rhodamine123 (Sigma-Aldrich, R8004) and 200 nM MitoTracker Green FM (InvitrogenTM, M7514) in incomplete media for 30 minutes in the incubator. After 3 washes with 1x dPBS for 5 minutes each, cells were observed by Zeiss Axio M2 Imager confocal laser scanning microscope. Laser power was set to 2 percent, pinhole size was set to 1 Airy unit, digital gain was set to 0.8-1.2, and master gain was set to 500-850 at all experiments. Images were acquired at a 1024 x 1024 (Rhodamine123-stained images) or a 512 x 512 frame size (MitoTracker Green FM-stained images) with a 8 bit depth by bi-directional scanning.

DAPI stock (20 mg/ml) was prepared by dissolving 10 mg of DAPI in 0.5 ml of dH₂O which was further diluted 1:100 fold in incomplete media to a concentration of 200 µg/ml. 25 µl of 200 µg/ml DAPI was applied to cells in a final volume of 1 ml.

Rhodamine123 stock (1 mg/ml) was prepared by dissolving 25 mg of Rhodamine123 in 25 ml of dH₂O. 5 µl of 1 mg/ml Rhodamine123 was applied to cells in a final volume of 1 ml. Lyophilized MitoTracker Green FM was dissolved in 74 µl of DMSO to a final concentration of 1mM. It was diluted 1:100 fold in incomplete media to a concentration of 1 µM. 200 µl of 1 µM MitoTracker Green FM was applied to cells in a final volume of 1 ml. All materials were equilibrated to room temperature before using.

2.7. QUANTITATIVE ANALYSIS OF CONFOCAL MICROSCOPY IMAGES

The raw image files in the .czi format were opened in the ZEISS ZEN Lite Black 2.3 SP1 software. Circles of same size were drawn in the mitochondrial area, nuclear area, and the cytoplasmic area. The signals were obtained from the “Measure” tab and transferred to a Microsoft Excel file. Each mitochondrial signal was subtracted from the average of the nuclear and cytoplasmic signals, then averaged for each experiment. The background subtracted and averaged values of all samples (control and FCCP-treated) obtained from three experiments were divided to the average of background subtracted and averaged control signals, and multiplied by 100. The averages and standard deviations of the normalized values were calculated, and used to make a bar graph.

MMP was calculated by dividing the average of background subtracted and averaged Rhodamine123 signals to the average of background subtracted and averaged MitoTracker Green FM signals. Each of the control and FCCP-treated MMP values were divided to the average of control MMP value and multiplied by 100. The averages and standard deviations of the normalized values from three experiments were calculated, and used to make a bar graph.

2.8. FILTER AIDED SAMPLE PREPARATION

Cell pellets were suspended with 500 μ l of cell lysis buffer (2 percent SDS, 0.1 M DTT, 0.1 M Tris-HCl pH 8) and incubated at 95°C for 5-7 min. After cooling the lysates down to room temperature, the lysates were sonicated thrice for 20 seconds. The lysates were centrifuged at 14,000 g for 15 minutes.

The supernatants were transferred into 1.5 ml microcentrifuge tubes. The protein concentrations of the samples were determined by Qubit Protein Assay Kit (Invitrogen™, Q33211). Qubit Working Solution was prepared by diluting the Qubit Protein Reagent 1:200 fold in Qubit® Protein Buffer. 20 μ l of 1:5 diluted sample was mixed with 180 μ l of Qubit Working Solution in an assay tube and incubated for 15 minutes at RT. The protein amount in the samples were measured by the Qubit Fluorometer.

Each protein extract sample (100 μ g in 30 μ l) along with 200 μ l urea wash solution (UW) (8 M urea (Bio-Rad #1610730) in 0.1 M Tris-HCl pH 8.5) were added into 30 kDa filter units in 1.5 ml microcentrifuge tubes (Merck Millipore, MRCF0R030). The tubes were centrifuged at 10,000 g for 15 min. The flow-through was discarded. This step was repeated with 100 μ l UW. Afterwards, 50 μ l of 50 mM iodoacetamide (GE Healthcare, RPN6302) (prepared in 8 M UW) was added into each filter unit. The tubes were incubated without mixing for 20 min in the dark at room temperature. 50 μ l of 10 mM dithiothreitol (GE Healthcare, 17131801) (prepared in 8 M UW) was added to each filter unit. The tubes were incubated for 15 min in the dark and centrifuged at 10,000 g for 10 min. The flow-through was discarded. The tubes were washed with 100 μ l of UW and centrifuged at 10,000 g for 15 min. The flow-through was discarded. This wash step was repeated once. The tubes were washed with 100 μ l of ammonium bicarbonate solution (40 mM NH_4HCO_3 in 0.1 M Tris-HCl pH 8.5) and centrifuged at 10,000 g for 15 min. The flow-through was discarded. This wash step was repeated once. Ammonium bicarbonate solution (40 μ l) containing trypsin (Promega Gold, V5280) in a 1:100 enzyme to protein ratio was added to each filter unit. The tubes were incubated in wet chamber for 18 hours at 37°C. The filter units were transferred to new 1.5 ml microcentrifuge tubes. Samples were eluted by centrifuging at 10,000 g for 10 min followed by two washes with 100 μ l of ammonium bicarbonate solution, and centrifugation at 10,000 g for 10 min.

After turning the filter units upside down, the samples were eluted into the same tubes by following the same procedure as above. Next, the eluates were transferred into glass insert tubes. After measuring the absorbance of ammonium bicarbonate solution as blank at 205 nm, peptide concentration of each sample was measured. The measurements were performed by applying 1 μ l of each solution onto the Thermo Scientific™ NanoDrop™ 2000 device. The samples were evaporated totally at 45°C and finally resuspended with 20 μ l of 0.1 percent formic acid solution diluted in proteomics-grade water. The insert tubes were taken into glass vials and stored at 4°C until mass spectrometry application.

2.9. MASS SPECTROMETRY-BASED PROTEIN EXPRESSION ANALYSIS

Peptide samples in glass vials were analyzed by nanoLC-captivespray-qTOF-MS/MS (Thermo Dionex RSLC3000 coupled with Bruker Compact). The information of the samples was entered to the Hystar 3.2 program. The sample (600 ng in 1 μ l) was injected into the 75 μ m I.D. x 15 cm nano liquid chromatography column (Acclaim PepMap RSLC C18, 2 μ m, 100 Å) with a flow rate of 200 nl/min to be separated prior to entrance to the mass spectrometer. The peptides were separated by using acetonitrile and formic acid as the mobile phase (mobile phase A: 100 percent proteomics-grade water, 0.1 percent formic acid; mobile phase B: 100 percent acetonitrile, 0.1 percent formic acid). Subsequently, the peptides were analyzed according to their mass-to-charge ratio by the Bruker Compact mass spectrometry which had been controlled by the otoofcontrol 3.3 program.

In order to identify the proteins in the samples, the data which were stored in the .mgf files were analyzed by Mascot 2.4.1 via Biotools 3.2. Swiss-Prot database was used for protein identification. In order to measure the expression levels of these proteins, the raw data which were obtained as .d bruker files were opened in MaxQuant program. “Label free quantification” and “Bruker Q-TOF” options were selected. The human proteome (proteome ID: UP000005640) was uploaded to the program from the UniProt database. Except from the above, no parameter was changed and the analysis was performed. Intensity-based expression levels of the identified proteins were obtained from the “proteingroups.txt” file which was generated by MaxQuant. The quantitative data were further processed in Perseus program and converted to a heat map. Next, the sequences of the proteins identified in each sample were downloaded in .fasta format from the UniProt

database to be uploaded to Blast2GO program. In the Blast2GO program, the proteins in the samples were analyzed according to the biological process they are involved, the cellular component they are in, and the molecular function they possess. In addition, the pathways which the proteins take place in were downloaded from the KEGG database.

2.10. STATISTICAL ANALYSIS

Data are shown as mean \pm standard deviation of the mean. Confocal microscopy data are representatives of three independent experiments while western blot data are representatives of three technical replicates. All experimental data were analyzed by unpaired Student's t-test, using the data analysis package in Microsoft Excel. P-value was set to 0.05 to identify the statistical significance of the differences between samples.

3. RESULTS

3.1. CIRCADIAN EXPRESSION OF BMAL1

Serum shock-synchronized HepG2 cells were incubated in serum-free media until they were collected. Cells were sampled every 3 hours for a 24-hour period. Rhythmic expression of BMAL1 over a 24-hour period was detected by western blot assay (Figure 3.1).

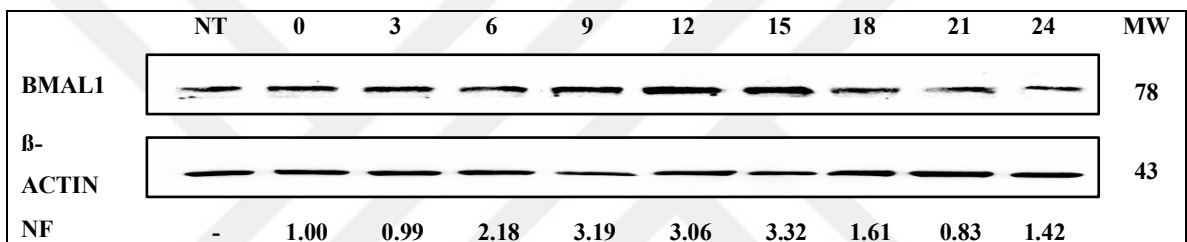


Figure 3.1. Representative blot of the circadian expression of BMAL1 in HepG2 cells (NT refers to the sample prior to serum shock, samples from 0-24 refers to each sample collected after serum shock with an interval of three hours, NF: normalization factor calculated with respect to β -ACTIN, MW: molecular weight in kilodaltons)

Subsequent western blot analyses demonstrated the oscillation pattern of BMAL1 levels in the HepG2 cell line (Figure 3.2). Cosinor analysis which enables to fit circadian data to a time series was performed to detect the timepoint at which BMAL1 peaks, in other words, the acrophase of BMAL1 expression. The analysis resulted in an acrophase of 11.58th hour in BMAL1 expression (Figure 3.3). For the following experiments, 12th hour was taken into consideration.

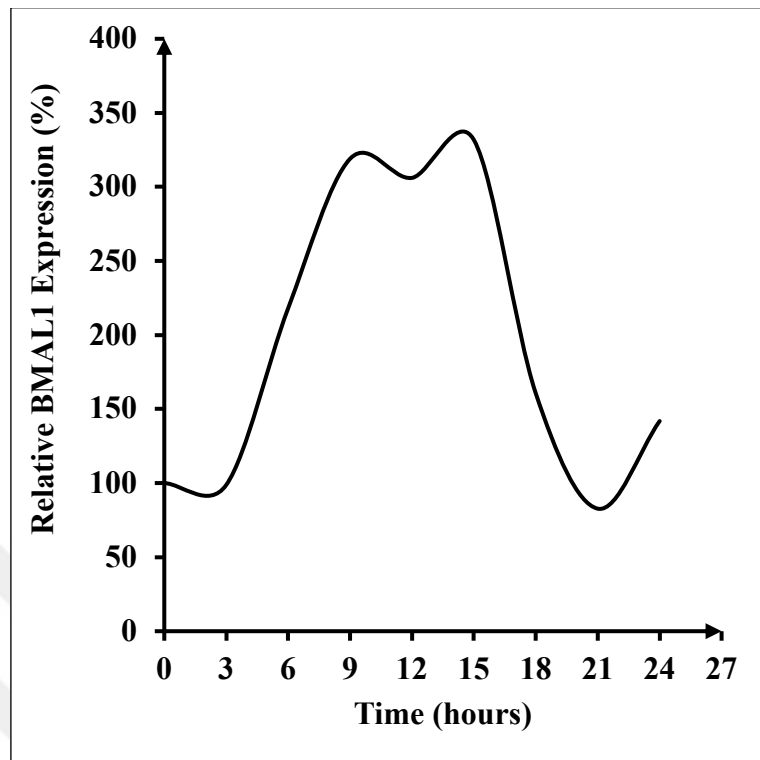


Figure 3.2. Rhythmic expression of BMAL1

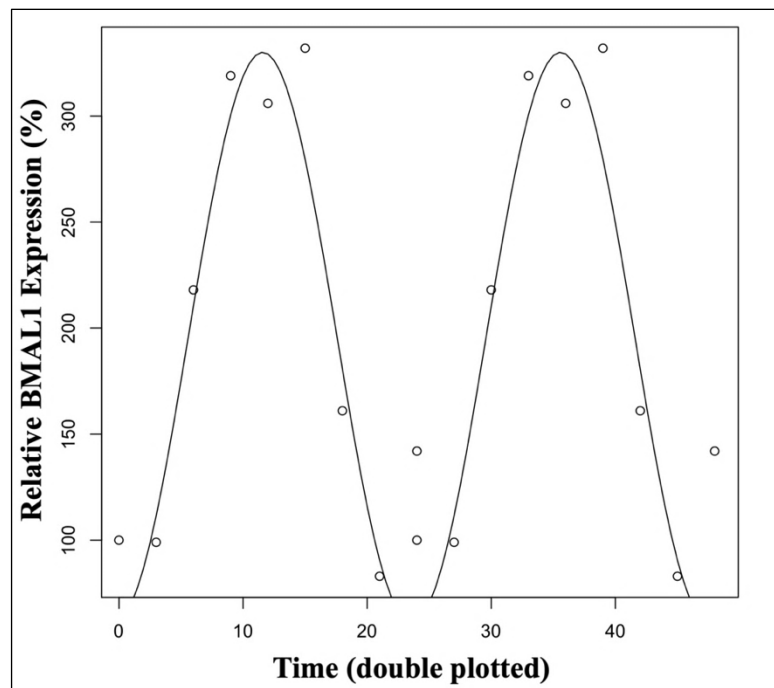


Figure 3.3. The acrophase of circadian BMAL1 expression

3.2. LIVE CELL IMAGING BY CONFOCAL LASER SCANNING MICROSCOPY: OPTIMIZATION FOR THREE FLUORESCENT DYES: DAPI, RHODAMINE123, MITOTRACKER GREEN FM

DAPI was utilized as a nuclear stain while Rhodamine123 and MitoTracker Green FM were used to stain mitochondria. DAPI is a cell impermeable blue fluorescent dye which stains nuclear DNA by binding to its minor groove. Rhodamine123 is a cell permeable, cationic green fluorescent dye which binds to the negative charges in the MMP. Therefore, it stains live mitochondria, only. MitoTracker Green FM is a cell permeable green fluorescent dye which binds to mitochondrial proteome. Thus, it can stain both live and dead mitochondria. Prior to conducting the experiments, a protocol for staining live cells by all three dyes was optimized. Since DAPI is a cell impermeable dye, different concentrations of DAPI (5 $\mu\text{g/ml}$ or 10 $\mu\text{g/ml}$) was applied to cells to see if the dye enters the cells. In this procedure, HepG2 cells were incubated with all three dyes together for 30 minutes in the incubator. After three washes of 5 minute each, the cells were imaged. In both samples, Rhodamine123 (5 $\mu\text{g/ml}$) and MitoTracker Green FM (200 nM) were imaged, yet, DAPI could not be imaged (Figure 3.4).

Next, the duration of DAPI incubation was extended from 30 minutes to two hours. After two hours of DAPI (5 $\mu\text{g/ml}$) incubation, the cells were briefly rinsed, and incubated with Rhodamine123 (5 $\mu\text{g/ml}$) and MitoTracker Green FM (200 nM) in either 1x dPBS (Figure, on the left) or serum-free media (Figure, on the right) for 30 minutes in the incubator. After three washes of 5 minute each, the cells were imaged. In both samples, all three dyes were observed. Because media is a safer option than PBS, serum-free media was used for all the incubations in the subsequent experiments (Figure 3.5).

Next, the protocol above was employed to detect MMP changes between control cells and FCCP (600 nM)-treated cells. However, a difference could not be detected as expected. Hence, the cells were stained with only Rhodamine123 to observe the changes in the MMP between control cells and FCCP-treated cells (Figure 3.6).

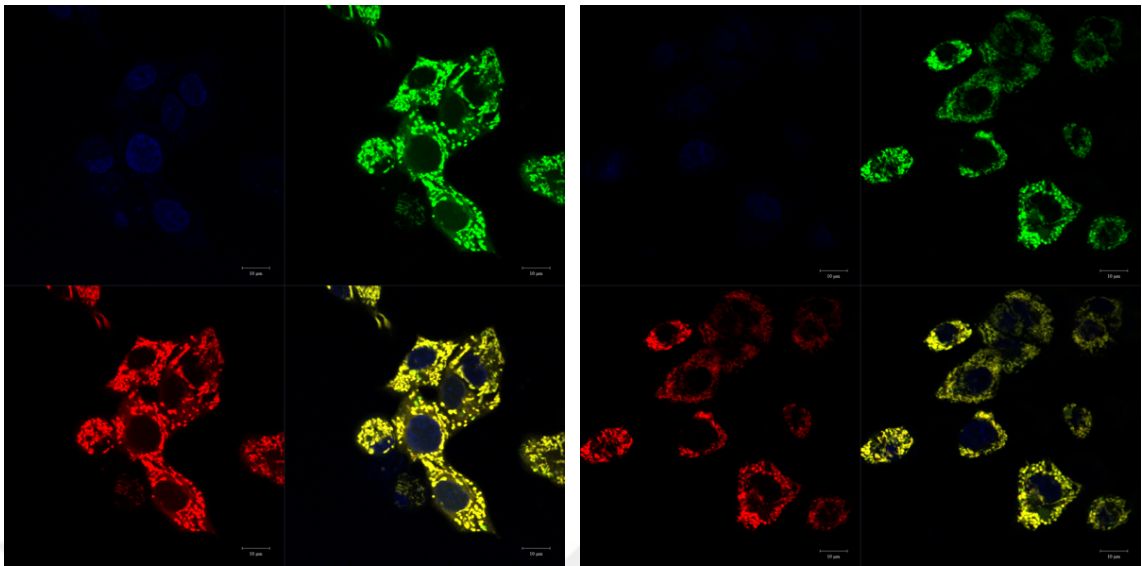


Figure 3.4. DAPI, Rhodamine123 and MitoTracker Green FM stained HepG2 cells (DAPI (5 µg/ml on the right, 10 µg/ml on the left) was applied to HepG2 cells along with Rhodamine123 (5 µg/ml) and MitoTracker Green FM (200 nM) for 30 minutes at 37°C)

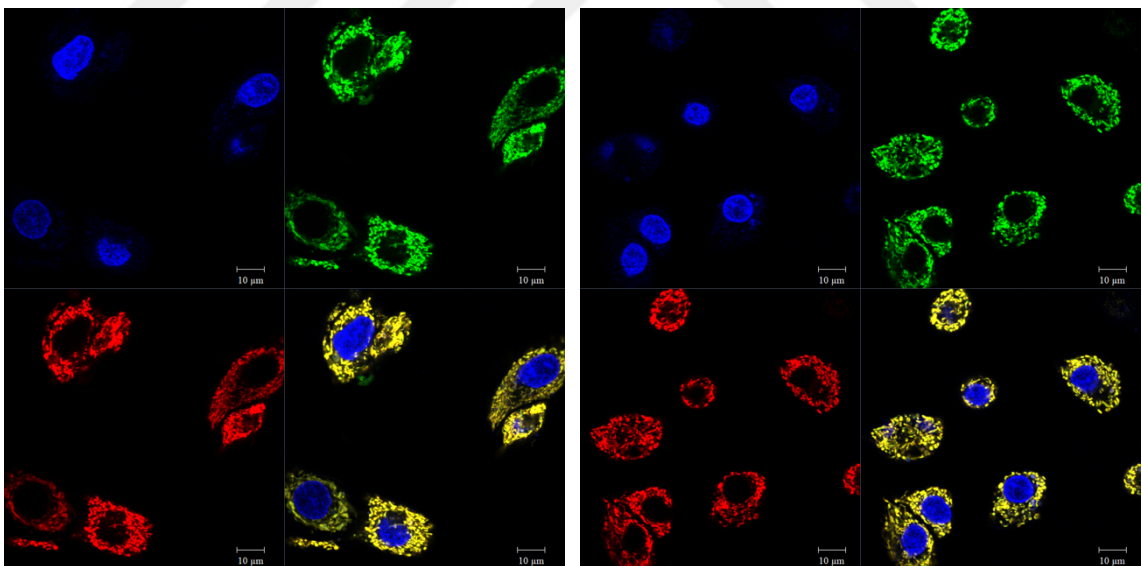


Figure 3.5. DAPI, Rhodamine123 and MitoTracker Green FM stained HepG2 cells (DAPI (5 µg/ml) was applied to HepG2 cells for two hours at 37°C. The cells were then incubated with Rhodamine123 (5 µg/ml) and MitoTracker Green FM (200 nM) in either 1x dpBS (on the left) or serum-free media (on the right) for 30 minutes at 37°C)

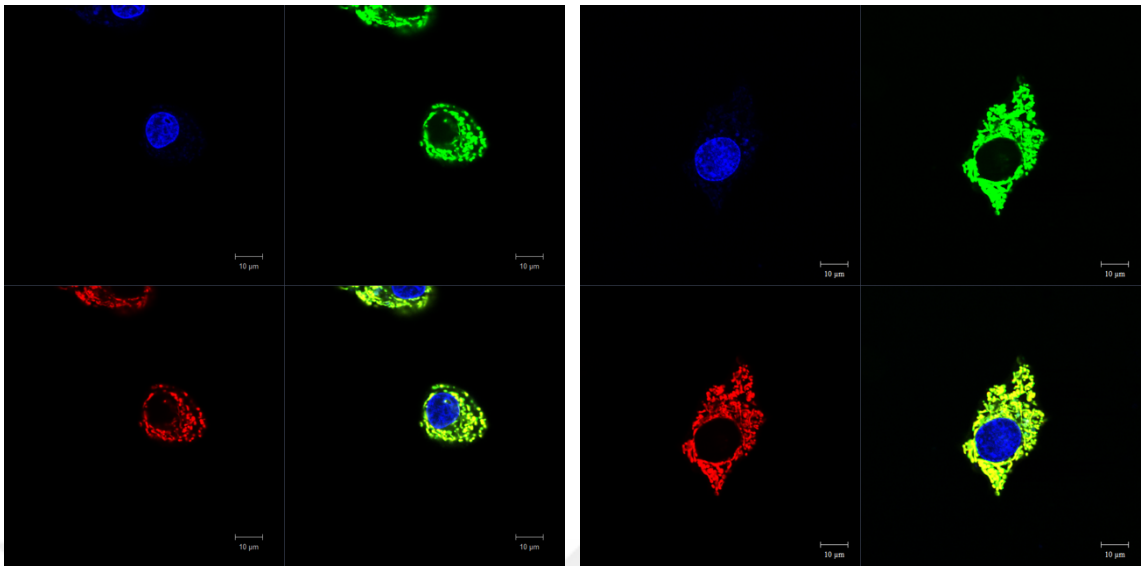


Figure 3.6. DAPI, Rhodamine123 and MitoTracker Green FM stained control and FCCP-treated HepG2 cells (Control (left) and FCCP (600 nM)-treated (right) (HepG2 cells were stained with DAPI (5 $\mu\text{g/ml}$) for 2 hours, Rhodamine123 (5 $\mu\text{g/ml}$) and MitoTracker Green FM (200 nM) for 30 minutes at 37°C)

3.3. MITOCHONDRIAL INNER MEMBRANE POTENTIAL ANALYSIS OF FCCP-TREATED CELLS BY USING RHODAMINE123 AND MITOTRACKER GREEN FM

Control HepG2 cells and FCCP (600 nM)-treated HepG2 cells were stained with Rhodamine123 (5 $\mu\text{g/ml}$) in order to observe MMP. In all three independent experiments, a diffused Rhodamine123 signal which indicated a disrupted MMP was observed in FCCP-treated cells compared to the non-treated group (Figure 3.7). The signals which were obtained from three independent experiments were quantified in the ZEN program. After subtracting the background signal from the mitochondrial signal, the mitochondrial signals were normalized to control. A 79 percent decrease in Rhodamine123 signal was detected in FCCP-treated sample with respect to the control sample. The decrease was statistically analyzed and found to be significant with a p-value of 0.003 (Figure 3.8).

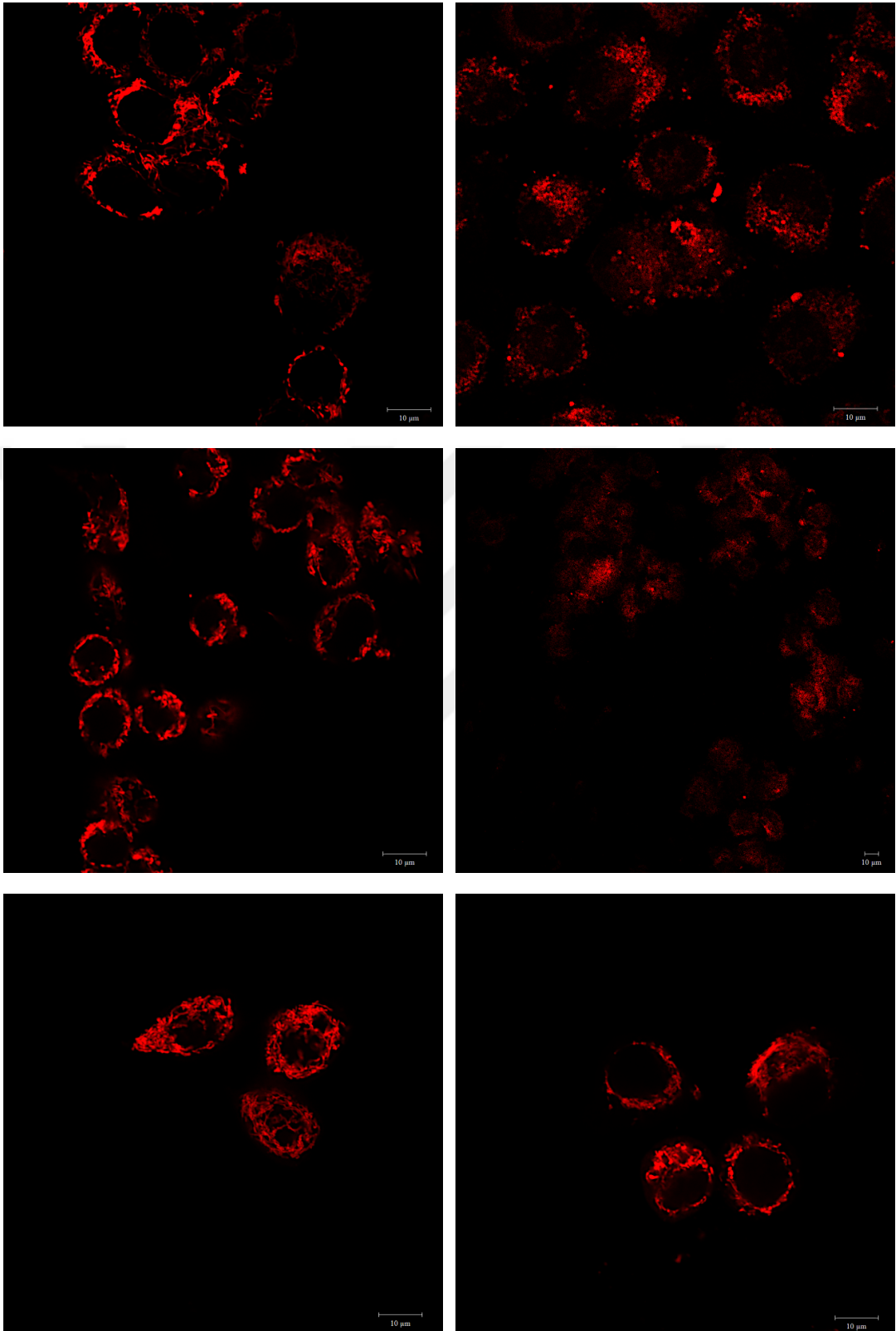


Figure 3.7. Rhodamine123 stained control (left) and FCCP-treated HepG2 cells (right) (HepG2 cells were stained with Rhodamine123 (5 µg/ml) for 30 minutes at 37°C)

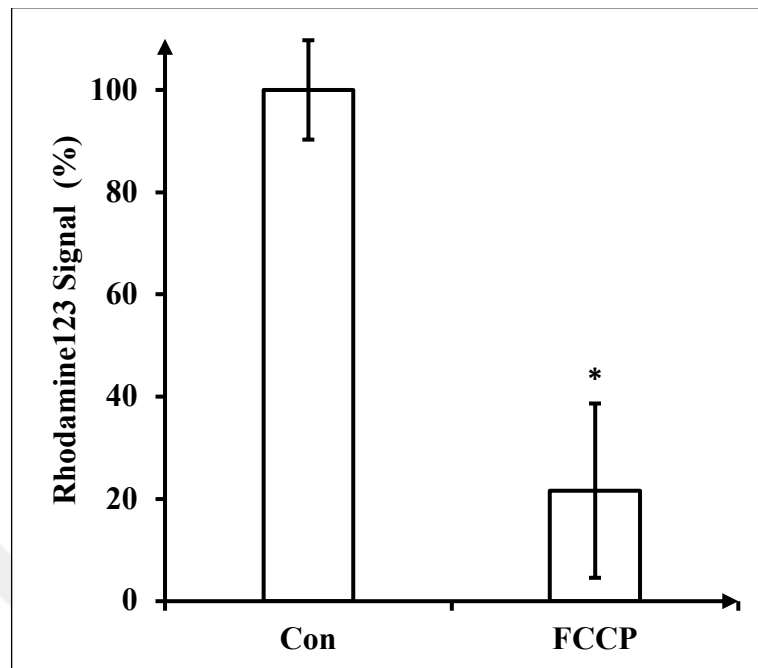


Figure 3.8. Quantitative Rhodamine123 signal in the control (Con) and FCCP-treated HepG2 cells (n =3, $p < 0.01$, *: significant difference with respect to the control)

In order to normalize the values obtained from Rhodamine123 staining to mitochondrial mass, control HepG2 cells and FCCP (600 nM)-treated HepG2 cells were dyed with MitoTracker Green FM (200 nM). In all three independent experiments, no change was observed in MitoTracker Green FM signals between control and FCCP-treated groups (Figure 3.9). The signals which were obtained from three independent experiments were quantified in the ZEN program. After subtracting the background signal from the mitochondrial signal, the mitochondrial signals were normalized to control. No significant change was detected the MitoTracker Green FM signals between control and FCCP-treated samples (Figure 3.10). MMP change was calculated by dividing the Rhodamine123 signal to the MitoTracker Green FM signal such that MMP was normalized to mitochondrial mass. As a result, a 79 percent decrease was observed in the MMP of FCCP-treated cells with respect the non-treated cells with a p-value of 0.003 (Figure 3.11).

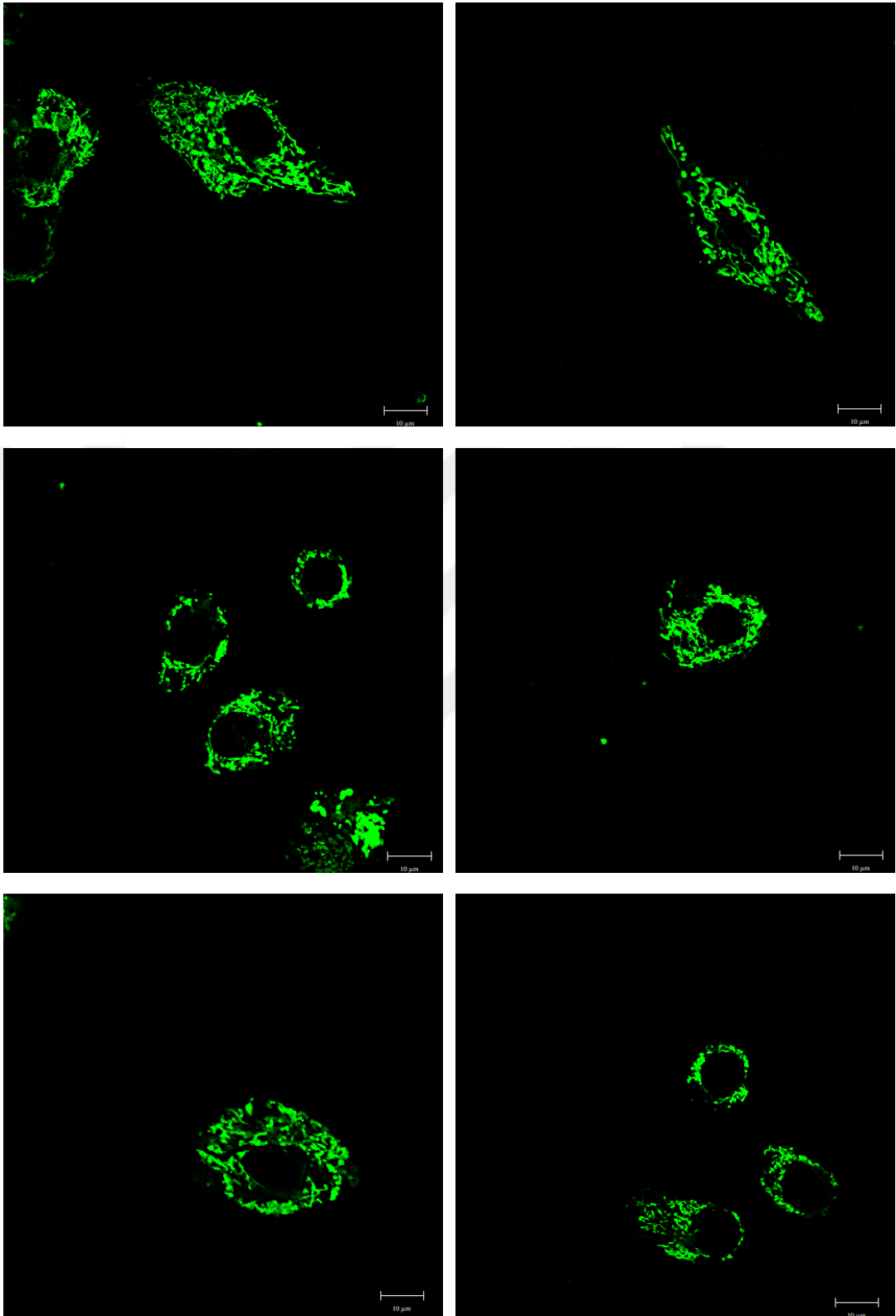


Figure 3.9. MitoTracker Gr FM stained control (left) and FCCP-treated HepG2 cells (right) (HepG2 cells were stained with MitoTracker Green FM (200 nM) for 30 minutes at 37°C)

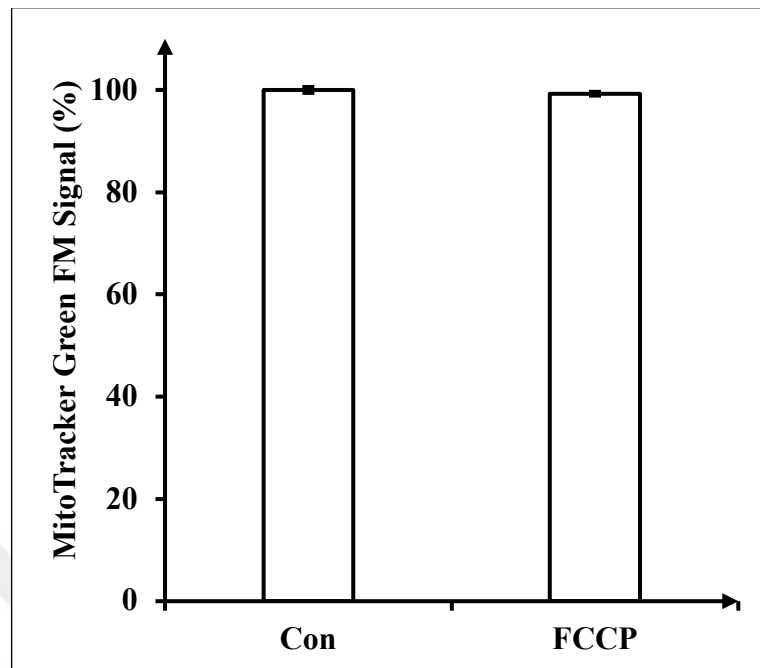


Figure 3.10. Quantitative MitoTracker Green FM signal in the control (Con) and FCCP-treated HepG2 cells

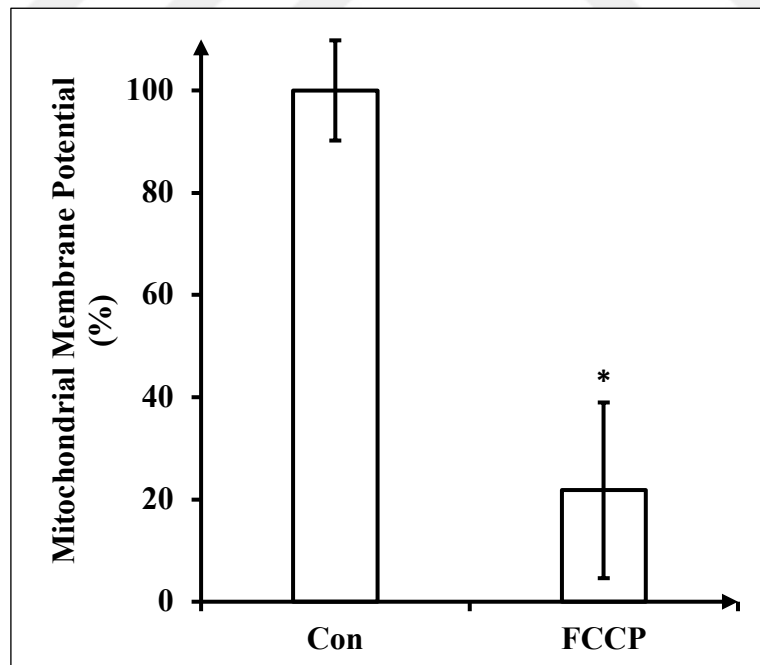


Figure 3.11. Mitochondrial inner membrane potential in the control (Con) and FCCP-treated (FCCP) HepG2 cells (n =3, p < 0.01, *: significant difference with respect to the control)

After the determination of the acrophase of BMAL1 expression, and the efficacy of FCCP treatment in the means of MMP change, the cells were treated with EX527 (50 mM) in order to inhibit specific SIRT1 activity. 16 hours of EX527 (50 mM) treatment was followed by the synchronization of the cells which was performed by two hours of serum shock with media comprising 50 percent FBS. The cells were incubated in the presence of either FCCP (600 nM), EX527 (50 mM) or both during serum shock. The cells were serum-starved with or without EX527 (50 mM) until sample collection at the acrophase of BMAL1 expression which was determined as 12th hour (circadian time 12, CT12) in the previous Cosinor analysis. The acetylation of control, FCCP-treated, EX527-treated, and co-treated cells at CT12 were investigated by western blot assay (Figure 3.12). Total acetylation signal of each blot was normalized to its respective β -ACTIN signal. Quantitative analysis of the three blots demonstrated significant changes in the acetylation levels of EX527- and co-treated samples with respect to control and FCCP-treated samples, respectively (Figure 3.13). While a 24 percent increase was detected in EX527-treated sample with respect to the non-treated group with a p-value of 0.048, a 31 percent increase was detected in co-treated sample with respect to FCCP-treated sample with a p-value of 0.039.

BMAL1 expression at CT12 in HepG2 cells was investigated by western blot assay (Figure 3.14). In FCCP-treated cells, BMAL1 levels were found to decrease drastically with respect to the control as expected. In both EX527- and co-treated cells, no visible change was observed in BMAL1 levels with respect to the non-treated group. BMAL1 signal of each blot was normalized to its respective β -ACTIN signal. Quantitative analysis of the three blots demonstrated significant changes in BMAL1 levels of FCCP-treated samples with respect to the control and co-treated samples (Figure 3.15). While a 63 percent decrease was detected in FCCP-treated sample with respect to the control with a p-value of 0.026, a 132 percent increase was detected in co-treated sample with respect to FCCP-treated sample with a p-value of 0.024. No significant change was detected in EX527- or co-treated samples with respect to the control.

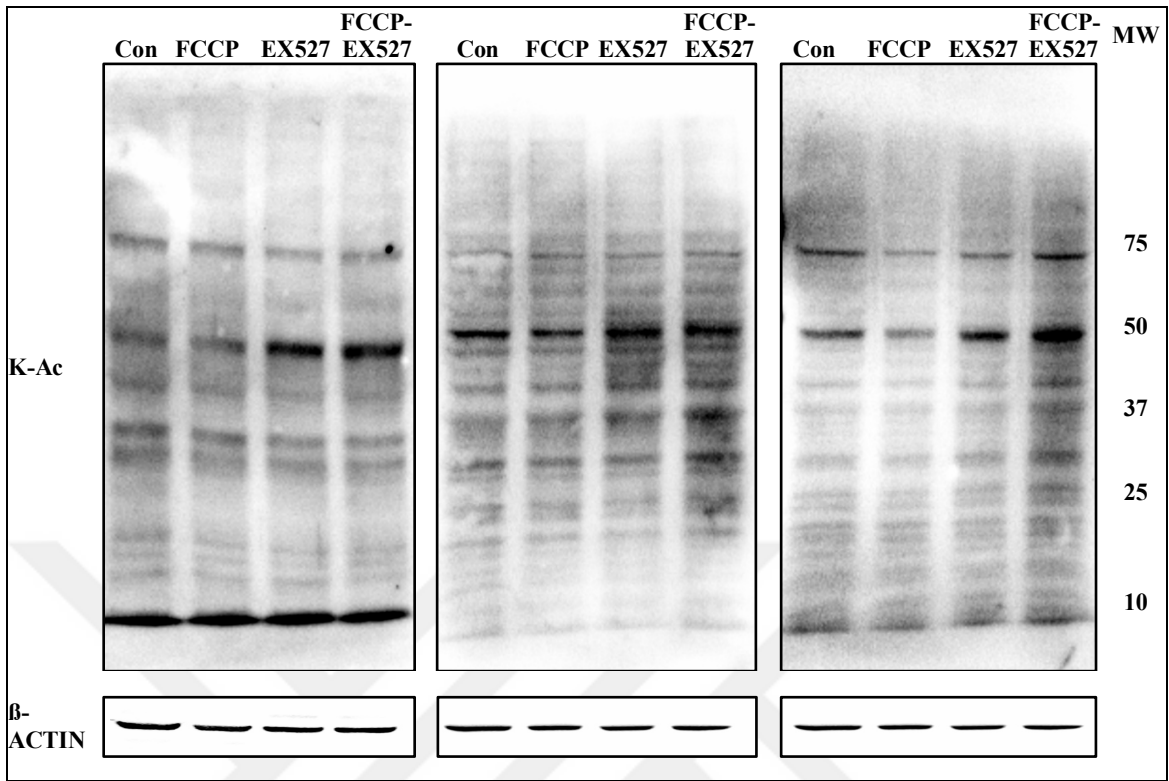


Figure 3.12. Total protein acetylation in the control (Con), FCCP-, EX527- or co-treated HepG2 cells at CT12 (MW: molecular weight in kDa)

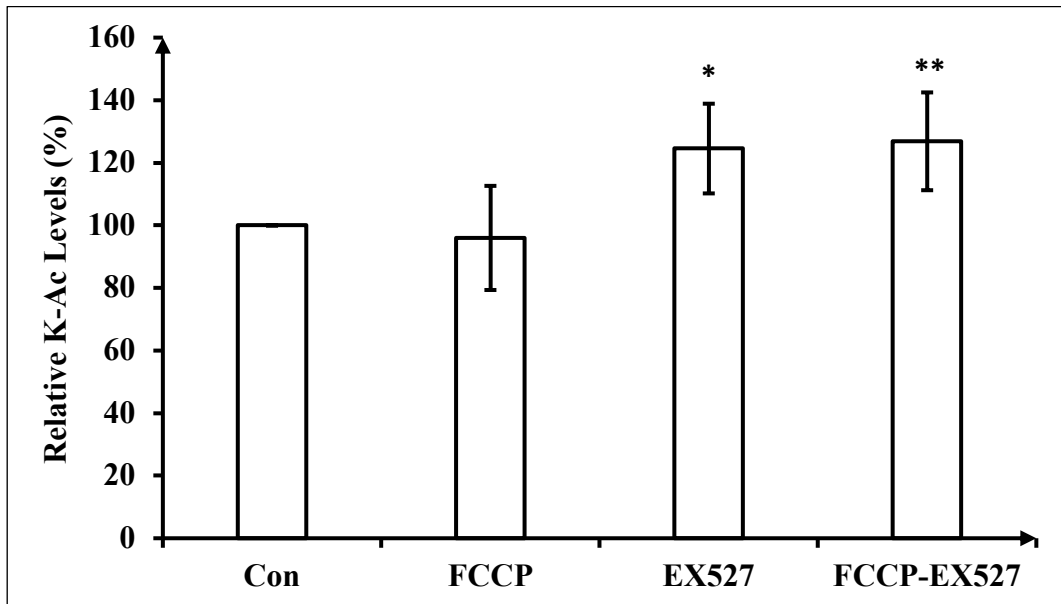


Figure 3.13. Quantitative analysis of total protein acetylation in the control (Con), FCCP-, EX527- or co-treated HepG2 cells at CT12 (n = 3, p < 0.05, *: significant difference with respect to the control, **: significant difference with respect to FCCP)

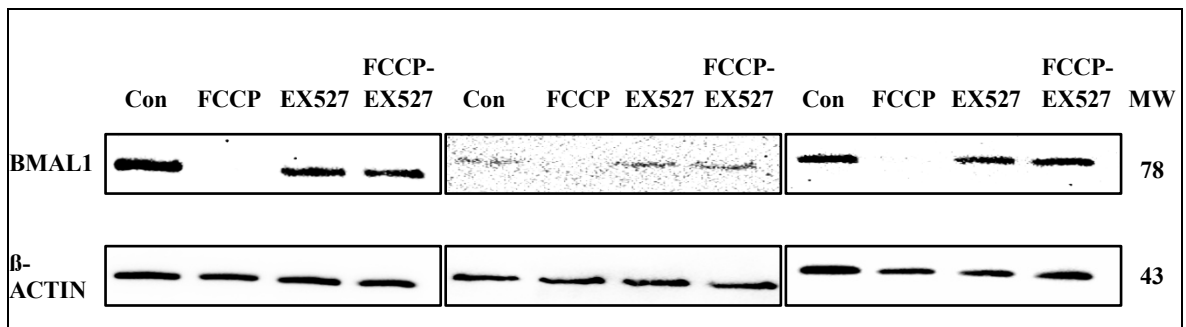


Figure 3.14. BMAL1 expression in the control (Con), FCCP-, EX527- or co-treated HepG2 cells at CT12 (MW: molecular weight in kDa)

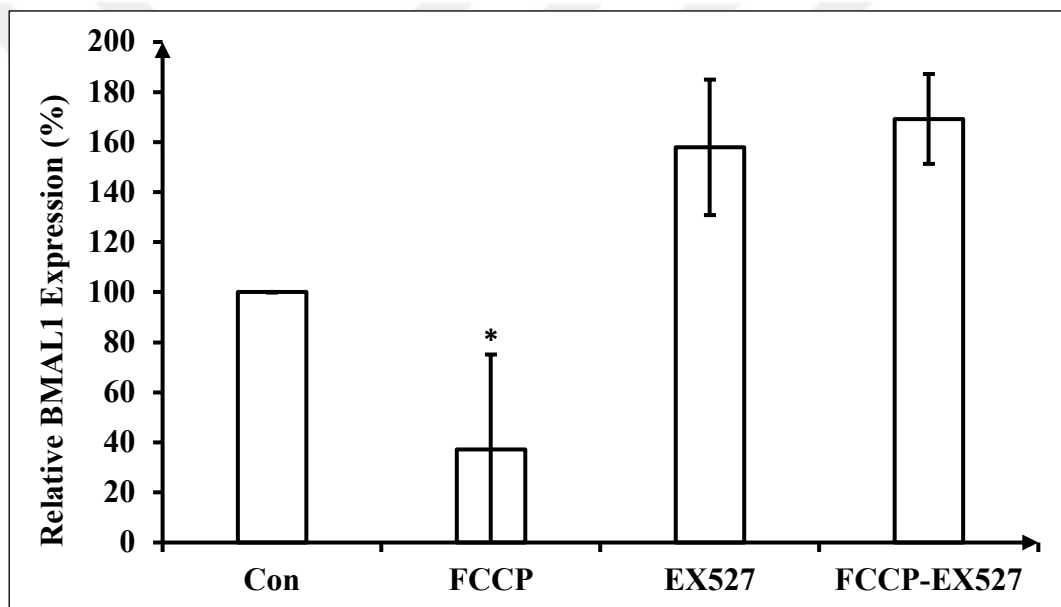


Figure 3.15. Quantitative analysis of BMAL1 expression in the control (Con), FCCP-, EX527- or co-treated HepG2 cells at CT12 (n =3, p < 0.05, * = significant difference with respect to the control, EX527, and FCCP-EX527)

3.4. ANALYSIS OF OXIDATIVE PHOSPHORYLATION COMPLEXES IN RESPONSE TO FCCP/EX527/CO- TREATMENT

In order to determine the metabolic effects FCCP and/or EX527 treatment in HepG2 cells at CT12, the levels of OXPHOS complexes were investigated by western blot assay (Figure 3.16). No significant change was determined in complex III (coenzyme

Q:cytochrome *c* oxidoreductase) or complex I (NADH dehydrogenase) with FCCP and/or EX527 treatment in subsequent quantitative western blot analysis (Figure 3.17).

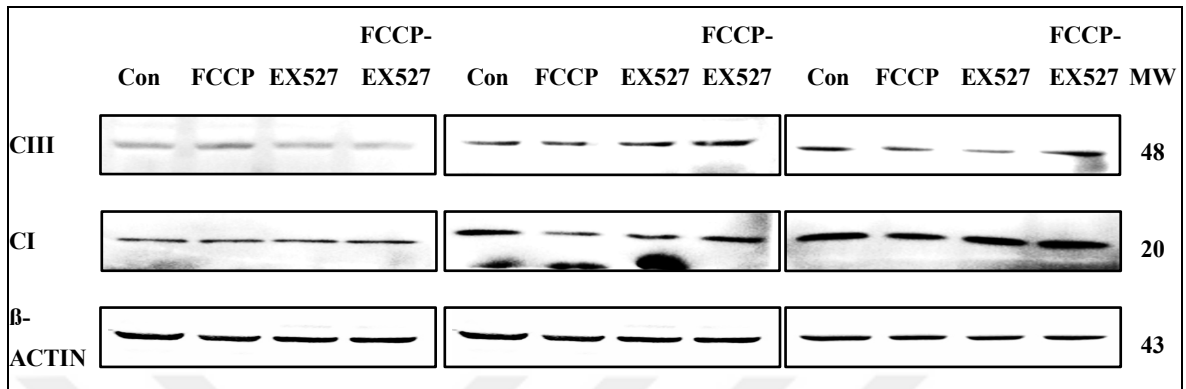


Figure 3.16. OXPHOS protein expression in the control (Con), FCCP-, EX527- or co-treated HepG2 cells at CT12 (Con: control, CIII: coenzyme Q:cytochrome *c* oxidoreductase, CI: NADH dehydrogenase, MW: molecular weight in kDa)

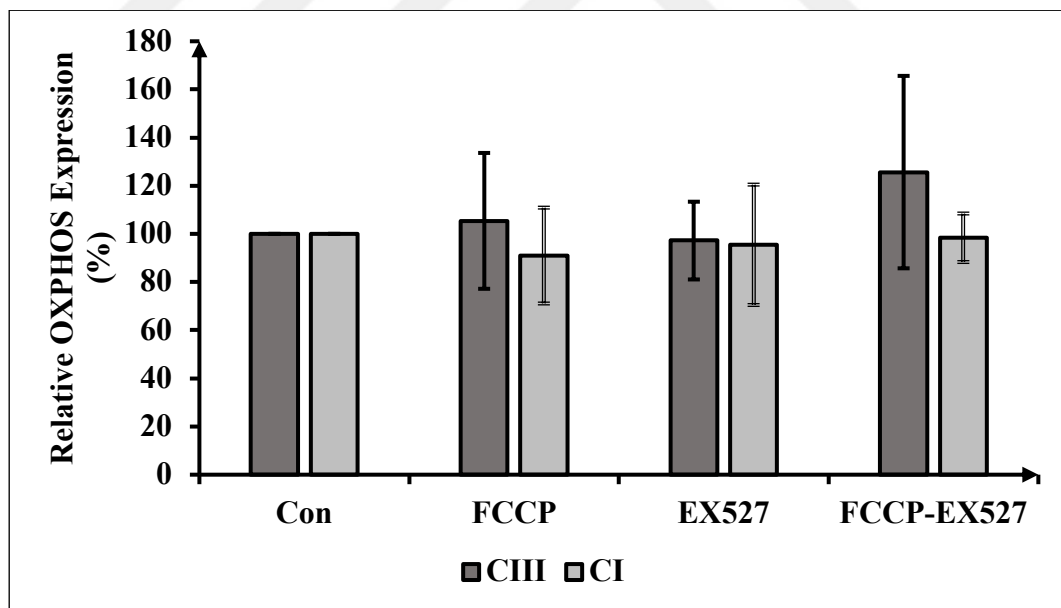


Figure 3.17. Quantitative analysis of OXPHOS protein expression in the control (Con), FCCP-, EX527- or co-treated HepG2 cells at CT12 (Con: control, n=3, CIII: coenzyme Q:cytochrome *c* oxidoreductase, CI: NADH dehydrogenase)

4. DISCUSSION

The aim of the study was to enlighten the unknown relationship between FCCP-induced mitochondrial inner membrane depolarization and BMAL1 downregulation. In FCCP-uncoupled HepG2 cells, BMAL1 expression was reported to be downregulated significantly. However, the feedback mechanism from the MMP disruption to BMAL1 downregulation has not been elucidated. In this study, it was found that EX527 treatment restores FCCP-induced BMAL1 downregulation in HepG2 cells, which indicates that SIRT1 activity is related with BMAL1 downregulation in response to the mitochondrial membrane depolarization induced by FCCP.

In order to uncover the changes in BMAL1 expression in a precise manner, the acrophase of BMAL1 expression was first determined by western blot and Cosinor analyses. The circadian expression of BMAL1 was obtained through western blot assay followed by the synchronization of HepG2 cells via serum shock, which is a well-established technique for circadian synchronization of cultured cells including HepG2 cell line. Serum shock synchronization which involves the incubation of cells with 50% FBS-containing media was proved to reset the circadian clock of the cells via the signaling molecules as well as the serum factors in the FBS. After resetting, the synchronized circadian clock of the cells can generally proceed for 72 hours. Circadian synchronization of the cells is commonly checked by transcriptional analysis of immediate-early genes such as *dbp*, *tef* or *per1*, which exhibit rhythmic expression. Protein expression analysis of the clock proteins can also be performed to prove circadian synchronization [111]. Since the expression of BMAL1 protein was investigated in this project, the synchronization of the circadian clock in HepG2 cells was validated by western blot analysis. Given that BMAL1 level peaks once a day at the circadian night as it becomes transcriptionally inactive [93], the single acrophase of BMAL1 expression can be stated as a consistent finding with the literature (Figure 3.1). The peaking time, in other words, the acrophase of BMAL1 expression was calculated by Cosinor analysis which uses the method of least squares in linear algebra in order to fit circadian data to a time series [112]. By using the quantitative western blot data in Cosinor analysis, the acrophase of BMAL1 expression in synchronized HepG2 cells was determined to be CT12 (Figure 3.2) which constitutes a consistent finding with the literature, as well [7]. Next, MMP was analyzed to investigate the uncoupling mediated by

FCCP in HepG2 cells. FCCP is an uncoupling agent which can induce mitochondrial membrane depolarization when used at an effective concentration. FCCP treatment at certain concentrations induces NADH oxidation by complex I, thus, increases oxygen consumption rate in the cells. The concentration at which FCCP maximizes oxygen consumption rate in HepG2 cells was determined as 600 nM [113]. Therefore, the cells were subjected to 600 nM of FCCP to induce mitochondrial uncoupling. Rhodamine123 was applied to cells to observe the influence of FCCP on MMP. Rhodamine123 is a cationic dye which binds to the negative MMP of mitochondria [114]. Hence, it requires live mitochondria to form interactions with. Live cell imaging of HepG2 cells revealed that Rhodamine123 diffused from the mitochondria into the cytosol and extracellular environment as its signal localized in the mitochondria significantly decreased with FCCP treatment (Figures 3.7, 3.8), indicating a disrupted MMP [115]. In order to examine mitochondrial mass [116], cells were stained with MitoTracker Green FM which binds to mitochondrial proteome from free thiol groups of cysteines. MitoTracker Green FM-staining did not reveal any change between the control and FCCP-treated samples (Figures 3.9, 3.10). Therefore, FCCP did not have any effect on neither mitochondrial proteome nor mitochondrial morphology. MMP *per se* was calculated by dividing the Rhodamine123 signal to the MitoTracker Green FM signal, so that the MMP was normalized to mitochondrial mass. As a result, a 79 percent decrease was calculated in the MMP with FCCP treatment in HepG2 cells (Figure 3.11). Additionally, mitochondria were in a dynamic and functional state in both samples since their morphologies in both conditions did not display a hyperfused or fragmented state which indicates increased or impaired OXPHOS, respectively [117]. Therefore, it can be asserted that FCCP treatment did not have an impact on mitochondrial functionality even though it disrupted MMP. Furthermore, the cells were dyed with DAPI so as to demonstrate that the cells remained intact during the experimental procedures; however, DAPI cannot penetrate live cells effectively due to its cell impermeable property [118]. Though two hours of DAPI incubation successfully stained HepG2 cells, it masked the effects of FCCP when it was applied along with Rhodamine123 and MitoTracker Green FM. Thus, Rhodamine123 and MitoTracker Green FM staining were applied, only.

After determining the effects of FCCP on mitochondria, cells were subjected to EX527 in order to inhibit specific SIRT1 activity. In the previous studies, 50 μ M EX527 had been

identified as an effective concentration to inhibit SIRT1 [119]. Total protein acetylation profile was investigated in all samples (FCCP-, EX527-, and co-treated) to discover the impact of SIRT1 inhibition on protein acetylation. As expected, EX527-treated samples exhibited a significant increase (24 percent and 31 percent) in total acetylation profile relative to their respective controls due to lack of SIRT1 deacetylase activity (Figures 3.12, 3.13). While being significant, EX527-treated samples did not lead to drastic changes in total acetylation profile, probably due to limited impact of SIRT1 on global lysine acetylation. The majority of acetylation sites (2911) were reported to reside in the nucleus, mostly being histones [120]. However, the histones were not detected due to their low molecular weight and the experimental setup that had been used. On the other hand, 2680 of acetylation sites were reported to reside in the mitochondria [120], which leads to the assumption that the total acetylation profile obtained was mostly mitochondrial. Nuclear fractionation could be executed to particularly observe the effects of EX527 on SIRT1 activity since SIRT1 is mainly localized in the nucleus [110].

Next, BMAL1 expression was investigated in response to FCCP and/or EX527 treatment. Significant downregulation of BMAL1 (63 percent) was detected in FCCP-treated samples relative to control by western blot assay (Figures 3.14, 3.15), as expected [7]. On the other hand, BMAL1 levels were found to be compatible in control, EX527- and co-treated samples, indicating that EX527 treatment only restored FCCP-induced downregulation of BMAL1, and did not trigger an extra response which could upregulate BMAL1 expression. The molecular link between mitochondrial membrane depolarization and SIRT1 activation could possibly involve the changes in mitochondrial redox status. NADH oxidation by complex I (NADH dehydrogenase) is known to be upregulated in response to membrane depolarization to restore its potential back [84]. As a result of NADH oxidation, mitochondrial NAD^+ concentration increases. It is not known whether the increase in mitochondrial NAD^+ can activate nuclear SIRT1 since subcellular NAD^+ pools are distinct from each other [121]. Moreover, it is not known whether the alterations in NAD^+ and NADH presence in different cellular compartments are perceivable among each other due to experimental limitations [122]. On the other hand, mitochondrial sirtuins (SIRT3-5) can be readily activated in response to mitochondrial NAD^+ buildup. In fact, the increase of mitochondrial NAD^+/NADH ratio, as a result of NADH dehydrogenase activity, was reported to activate SIRT3 [123]. Consequently, it can be assumed that mitochondrial

NAD⁺ increase can lead to SIRT1 activation. However, this assumption needs further investigation, such as measuring NAD⁺/NADH ratio and specific SIRT1 activity in response to FCCP treatment. Another implication of mitochondrial membrane depolarization is the increment of AMP/ATP ratio in the mitochondria as ATP synthase cannot function due to uncoupling [5]. Increased AMP/ATP ratio is a known activator of AMP-activated protein kinase (AMPK). Activated AMPK was found to trigger cytosolic SIRT1 activity by mediating an increment in NAD⁺/NADH ratio in the cytosol. Therefore, it is also probable that SIRT1 can bind to BMAL1:CLOCK in the cytosol causing BMAL1 deacetylation, and enable the BMAL1:CLOCK dimer enter the nucleus to perform their transcriptional activity as it is the case with PGC1- α and FOXO3a [124]. The link between SIRT1-mediated deacetylation of BMAL1 and BMAL1 degradation could be readily established since acetylation of BMAL1 inactivates the transcriptional activity of BMAL1:CLOCK dimer. Inactive BMAL1:CLOCK dimer is more stable than its transcriptionally active state. In its active state, BMAL1:CLOCK dimer is rapidly sumoylated, ubiquitinated, and finally degraded via proteasomal-degradation pathway after it recruits transcription factors to the promoter region of the DNA. Afterwards, another BMAL1:CLOCK dimer is recruited to the E-box to enhance the expression of the clock-controlled genes. When BMAL1 is acetylated, transcriptional activity of BMAL1:CLOCK dimer is inhibited, thus, BMAL1:CLOCK dimer is not prone to proteasomal degradation via the sequential modifications mentioned above [25]. Hence, it can be deduced that SIRT1 inhibition prevented BMAL1 degradation by rendering it more stable than its deacetylated state. The posttranslational modifications on BMAL1 in response to FCCP/EX527 treatment should be identified separately in order to ascertain whether this hypothesis is true. Immunoprecipitation of BMAL1 can be performed for subsequent western blot assays against protein acetylation and/or ubiquitination in order to identify the posttranslational modifications on BMAL1 in response to FCCP/EX527 treatment.

Alternatively, FCCP/EX527 treatment could have led to proteomic changes in HepG2 cells that would influence BMAL1 expression or BMAL1 stability. For instance, ribonucleic acid complex I (RAE1) and nucleoporin 98kDa (NUP98) proteins that have recently been established as the promoters of BMAL1 degradation, could be linked to FCCP/EX527-mediated regulation of BMAL1 [125]. Other than these candidates, novel proteins that influence BMAL1 levels can be discovered via mass spectrometry-based protein

expression analysis of FCCP/EX527-treated samples which are collected at different timepoints. By doing so, the proteomic changes in the cells due to the treatments can be analyzed in a time-dependent manner which will eventually help uncovering the actors, thus, the pathways behind differential BMAL1 regulation. The effects of the candidate proteins on BMAL1 levels can be further investigated through genetic manipulations of these proteins, such as knockdown or knockout techniques.

Finally, the metabolic effects of FCCP/EX527 treatment was investigated by analyzing the expression levels of OXPHOS proteins. The expression levels of oxidative phosphorylation complexes III (coenzyme Q:cytochrome *c* oxidoreductase) and I (NADH dehydrogenase) were not changed in response to FCCP/EX527 treatment (Figures 3.16, 3.17). It should be noted for OXPHOS immunoblotting assays that detection of all complexes might be limited due to their relative amounts in whole cell lysates. These samples can be enriched for the OXPHOS complexes in order to unveil the effects of those treatments on OXPHOS. Additionally, the activities of each complex should be measured to unveil the effects of FCCP/EX527 treatment on mitochondrial functionality. In-gel complex activity assays, oxygen consumption rate or ATP synthase activity measurements can be conducted to examine if FCCP/EX527 treatments rendered the cells metabolically inactive. Nonetheless, the activity of the ETC complexes would probably be upregulated in response to FCCP treatment while the activity of ATP synthase would be downregulated due to uncoupling of OXPHOS. In addition, EX527-induced SIRT1 inhibition would alter OXPHOS activity since SIRT1 has been established as a promoter of PGC1- α -mediated mitochondrial biogenesis [124]. Though, it should be noted that the downregulatory effects of SIRT1 inhibition on OXPHOS activity cannot be immediately detected since the half-lives of the complexes are relatively long, ranging from two days up to nine days [126,127].

5. CONCLUSIONS AND FUTURE PERSPECTIVE

The circadian clock times the behavior, physiology, and metabolism of a wide array of species. The reciprocal relation between the circadian clock and metabolism have extensively been researched since circadian rhythm disruptions take part in the pathology of numerous diseases in which mitochondria also have a crucial role as the powerhouse of the cells. While the majority of the research have investigated the genetic basis of this relationship, functional implications of this relationship are yet to be illuminated, such as the impacts of mitochondrial functionality or mitochondrial redox on the regulation of the circadian clock.

In this study, the molecular mechanism behind the changes in BMAL1 expression in response to FCCP-mediated mitochondrial membrane depolarization was aimed to be elucidated. It was found that SIRT1 inhibition restores FCCP-induced downregulation of BMAL1. However, the link between FCCP-induced mitochondrial membrane depolarization and SIRT1 activation remains to be solved as NAD⁺ sensing between distinct cellular compartments cannot be conclusively determined due to lack of advanced techniques. While the relationship between the circadian clock and SIRT1 is well-established in terms of rhythmic regulation of BMAL1:CLOCK transcriptional activity, deacetylation of both BMAL1 and PER2 by SIRT1 remains controversial as the two processes yield two contradictory outcomes. Alternatively, the proteomic changes in response to FCCP/EX527 treatment can provide an insight to the pathway where BMAL1 is downregulated in response to FCCP treatment. Lastly, the vast number of modifications associated with the molecular clock, nucleocytoplasmic shuttling, transactivation, and degradation pathways of BMAL1:CLOCK dimer renders the regulation of the circadian clock rather elusive.

The regulation of the circadian clock is of capital importance due to its strong influence on health. Given that the molecular processes involved in the "absorption, distribution, metabolism, and excretion" of drugs are directly or indirectly regulated by the circadian clock, the timing of drug administration actually influences the efficiency of drug-based therapies. Chronotherapy-based approaches have become prevalent to fight diseases in a more effective and less detrimental way.

Finally, maintaining a functional circadian clock not only enables one to “run like clockwork”, it also helps preventing diseases, and fighting them when coupled with the righteous therapy. Events that threaten the integrity of the circadian clock, including the mitochondrial ones, deserve more attention.



REFERENCES

1. Takahashi JS, Shimomura K, Kumar V, Benzer S. Searching for genes underlying behavior: lessons from circadian rhythms. *Science*. 2008;322(5903):909–11.
2. Aschoff J, Fatranska M, Giedke H. Human circadian rhythms in continuous darkness: entrainment by social cues. *Science*. 1970;17(5):213–5.
3. Refinetti R, Menaker M. The circadian rhythm of body temperature. *Frontiers in Bioscience*. 2010;15(3):564–94.
4. Weitzman ED. Circadian rhythms and episodic hormone secretion in man. *Annual Review of Medicine*. 1976;27:225–43.
5. Mitchell P. Chemiosmotic coupling in oxidative and photosynthetic phosphorylation. *Biochimica et Biophysica Acta - Bioenergetics*. 2011;1807(12):1507–38.
6. Benz R, McLaughlin S. The molecular mechanism of action of the proton ionophore fccp (carbonylcyanide p-trifluoromethoxyphenylhydrazone). *Biophysical Journal*. 1983;41(3):381–98.
7. Scrima R, Cela O, Merla G, Augello B, Rubino R, Quarato G, et al. Clock genes and mitochondrial respiratory activity: evidence of a reciprocal interplay. *Biochimica et Biophysica Acta - Bioenergetics*. 2016;1857(8):1344–51.
8. Dibner C, Schibler U, Albrecht U. The mammalian circadian timing system: organization and coordination of central and peripheral clocks. *Annual Review of Physiology*. 2010;72(1):517–49.
9. Pittendrigh CS. Circadian rhythms and the circadian organization of living systems. *Cold Spring Harbor Symposia on Quantitative Biology*;1960.
10. Do MTH, Yau K-W. Intrinsically photosensitive retinal ganglion cells. *Physiological Reviews*. 2010;90(4):1547–81.
11. Buijs RM, Kalsbeek A. Hypothalamic integration of central and peripheral clocks. *Nature Reviews Neuroscience*. 2001;2(7):521–6.

12. Balsalobre A, Brown SA, Marcacci L, Tronche F, Kellendonk C, Reichardt HM, et al. Resetting of circadian time in peripheral tissues by glucocorticoid signaling. *Science*. 2000;289(5488):2344–7.
13. Boivin DB, James FO, Wu A, Cho-Park PF, Xiong H, Sun ZS. Circadian clock genes oscillate in human peripheral blood mononuclear cells. *Blood*. 2003;102(12):4143–5.
14. Brown SA, Zimbrunn G, Fleury-Olela F, Preitner N, Schibler U. Rhythms of mammalian body temperature can sustain peripheral circadian clocks. *Current Biology*. 2002;12(18):1574–83.
15. Damiola F, Le Minli N, Preitner N, Kornmann B, Fleury-Olela F, Schibler U. Restricted feeding uncouples circadian oscillators in peripheral tissues from the central pacemaker in the suprachiasmatic nucleus. *Genes and Development*. 2000;14(23):2950–61.
16. Lowrey PL, Takahashi JS. Genetics of the mammalian circadian system: photic entrainment, circadian pacemaker mechanisms, and posttranslational regulation. *Annual Review of Genetics*. 2000;34(1):533–62.
17. Gekakis N, Staknis D, Nguyen HB, Davis FC, Wilsbacher LD, King DP, et al. Role of the clock protein in the mammalian circadian mechanism. *Science*. 1998;280(5369):1564–9.
18. Rey G, Cesbron F, Rougemont J, Reinke H, Brunner M, Naef F. Genome-wide and phase-specific dna-binding rhythms of bmal1 control circadian output functions in mouse liver. *PLOS Biology*. 2011;9(2):e1000595.
19. Vitaterna MH, Selby CP, Todo T, Niwa H, Thompson C, Fruechte EM, et al. Differential regulation of mammalian period genes and circadian rhythmicity by cryptochromes 1 and 2. *Proceedings of the National Academy of Sciences*. 1999;96(21):12114–9.
20. Ye R, Selby CP, Chiou YY, Ozkan-Dagliyan I, Gaddameedhi S, Sancar A. Dual modes of clock:bmal1 inhibition mediated by cryptochrome and period proteins in the mammalian circadian clock. *Genes and Development*. 2014;28(18):1989–98.

21. Hastings MH, Maywood ES, Brancaccio M. Generation of circadian rhythms in the suprachiasmatic nucleus. *Nature Reviews Neuroscience*. 2018;19(8):453–69.
22. Sato TK, Panda S, Miraglia LJ, Reyes TM, Rudic RD, McNamara P, et al. A functional genomics strategy reveals rora as a component of the mammalian circadian clock. *Neuron*. 2004; 43(4):527-37.
23. Preitner N, Damiola F, Luis-Lopez-Molina, Zakany J, Duboule D, Albrecht U, et al. The orphan nuclear receptor rev-erb α controls circadian transcription within the positive limb of the mammalian circadian oscillator. *Cell*. 2002;110(2):251–60.
24. Triqueneaux G, Thenot S, Kakizawa T, Antoch MP, Safi R, Takahashi JS, et al. The orphan receptor rev-erb α gene is a target of the circadian clock pacemaker. *Journal of Molecular Endocrinology*. 2004;33(3):585–608.
25. Hirano A, Fu YH, Ptáek LJ. The intricate dance of post-translational modifications in the rhythm of life. *Nature Structural and Molecular Biology*. 2016;23(12):1053–60.
26. Witting W, Kwa IH, Eikelenboom P, Mirmiran M, Swaab DF. Alterations in the circadian rest-activity rhythm in aging and alzheimer's disease. *Biological Psychiatry*. 1990;27(6):563–72.
27. Song H, Moon M, Choe HK, Han DH, Jang C, Kim A, et al. A β -induced degradation of bmal1 and cbp leads to circadian rhythm disruption in alzheimer's disease. *Molecular Neurodegeneration*. 2015;10(1):13.
28. Videnovic A, Golombek D. Circadian and sleep disorders in parkinson's disease. *Experimental Neurology*. 2013;243:45–56.
29. Morton AJ. Disintegration of the sleep-wake cycle and circadian timing in huntington's disease. *Journal of Neuroscience*. 2005;25(1):157–63.
30. Musiek ES. Circadian clock disruption in neurodegenerative diseases: cause and effect? *Frontiers in Pharmacology*. 2015;6(29):1–6.
31. Bass J, Lazar MA. Circadian time signatures of fitness and disease. *Science*. 2016;354(6315):994–9.

32. Mongrain V, La Spada F, Curie T, Franken P. Sleep loss reduces the dna-binding of bmal1, clock, and npas2 to specific clock genes in the mouse cerebral cortex. *Plos One*. 2011;6(10):e26622.
33. Roman GW, Loh DH, Eckel-Mahan KL, Rawashdeh O, Wright KP, Lyons LC, et al. Cycling behavior and memory formation. *Journal of Neuroscience*. 2009;29(41):12824–30.
34. Craig LA, McDonald RJ. Chronic disruption of circadian rhythms impairs hippocampal memory in the rat. *Brain Research Bulletin*. 2008;76(1–2):141–51.
35. Kondratova AA, Dubrovsky Y V., Antoch MP, Kondratov R V. Circadian clock proteins control adaptation to novel environment and memory formation. *Aging*. 2010;2(5):285–97.
36. Kondratov R V., Kondratova AA, Gorbacheva VY, Vykhovanets O V., Antoch MP. Early aging and age-related pathologies in mice deficient in bmal1, the core component of the circadian clock. *Genes and Development*. 2006;20(14):1868–73.
37. Kuo S-J, Chen S-T, Yeh K-T, Hou M-F, Chang Y-S, Hsu NC, et al. Disturbance of circadian gene expression in breast cancer. *Virchows Archiv*. 2009;454(4):467–74.
38. Taniguchi H, Fernández AF, Setién F, Ropero S, Ballestar E, Villanueva A, et al. Epigenetic inactivation of the circadian clock gene bmal1 in hematologic malignancies. *Cancer Research*. 2009;69(21):8447–54.
39. Hsu C-M, Lin S-F, Lu C-T, Lin P-M, Yang M-Y. Altered expression of circadian clock genes in head and neck squamous cell carcinoma. *Tumor Biology*. 2012;33(1):149–55.
40. Røe OD, Anderssen E, Helge E, Pettersen CH, Olsen KS, Sandeck H, et al. Genome-wide profile of pleural mesothelioma versus parietal and visceral pleura: the emerging gene portrait of the mesothelioma phenotype. *Plos One*. 2009;4(8):1–15.
41. Taniguchi H, Fernández AF, Setién F, Ropero S, Ballestar E, Villanueva A, et al. Epigenetic inactivation of the circadian clock gene bmal1 in hematologic malignancies. *Cancer Research*. 2009;69(21):8447–54.

42. Tokunaga H, Takebayashi Y, Utsunomiya H, Akahira JI, Higashimoto M, Mashiko M, et al. Clinicopathological significance of circadian rhythm-related gene expression levels in patients with epithelial ovarian cancer. *Acta Obstetrica et Gynecologica Scandinavica*. 2008;87(10):1060–70.
43. Zhu Y, Stevens RG, Hoffman AE, FitzGerald LM, Kwon EM, Ostrander EA, et al. Testing the circadian gene hypothesis in prostate cancer: a population-based case-control study. *Cancer Research*. 2009;69(24):9315–22.
44. Katamune C, Koyanagi S, Shiromizu S, Matsunaga N, Shimba S, Shibata S, et al. Different roles of negative and positive components of the circadian clock in oncogene-induced neoplastic transformation. *Journal of Biological Chemistry*. 2016;291(20):10541–50.
45. Gibbs JE, Blaikley J, Beesley S, Matthews L, Simpson KD, Boyce SH, et al. The nuclear receptor rev-erb α mediates circadian regulation of innate immunity through selective regulation of inflammatory cytokines. *Proceedings of the National Academy of Sciences*. 2011;109(2):582–7.
46. Geyfman M, Kumar V, Liu Q, Ruiz R, Gordon W, Espitia F, et al. Brain and muscle arnt-like protein-1 (bmal1) controls circadian cell proliferation and susceptibility to uvb-induced dna damage in the epidermis. *Proceedings of the National Academy of Sciences*. 2012;109(29):11758–63.
47. Zeng ZL, Wu MW, Sun J, Sun YL, Cai YC, Huang YJ, et al. Effects of the biological clock gene bmal1 on tumour growth and anti-cancer drug activity. *Journal of Biochemistry*. 2010;148(3):319–26.
48. Sahar S, Sassone-Corsi P. Metabolism and cancer: the circadian clock connection. *Nature Reviews Cancer*. 2009;9(12):886–96.
49. Kang TH, Sancar A. Circadian regulation of dna excision repair: implications for chrono-chemotherapy. *Cell Cycle*. 2009;8(11):1665–7.
50. Filipski E. Host circadian clock as a control point in tumor progression. *Journal of National Cancer Institute*. 2002;94(9):690–7.
51. Gréchez-Cassiau A, Rayet B, Guillaumond F, Teboul M, Delaunay F. The circadian

- clock component *bmal1* is a critical regulator of p21 *waf1/cip1* expression and hepatocyte proliferation. *Journal of Biological Chemistry*. 2008;283(8):4535–42.
52. Mullenders J, Fabius AWM, Madiredjo M, Bernards R, Beijersbergen RL. A large scale shRNA barcode screen identifies the circadian clock component *arntl* as putative regulator of the p53 tumor suppressor pathway. *Plos One*. 2009;4(3).
 53. Van Cauter E, Polonsky KS, Scheen AJ. Roles of circadian rhythmicity and sleep in human glucose regulation. *Endocrine Reviews*. 1997;18(5):716–38.
 54. Hagström-Toft E, Bolinder J, Ungerstedt U, Arner P. A circadian rhythm in lipid mobilization which is altered in IDDM. *Diabetologia*. 1997;40(9):1070–8.
 55. Ando H, Yanagihara H, Hayashi Y, Obi Y, Tsuruoka S, Takamura T, et al. Rhythmic messenger ribonucleic acid expression of clock genes and adipocytokines in mouse visceral adipose tissue. *Endocrinology*. 2005;146(12):5631–6.
 56. Lamia KA, Storch K-F, Weitz CJ. Physiological significance of a peripheral tissue circadian clock. *Proceedings of the National Academy of Sciences*. 2008;105(39):15172–7.
 57. Huang N, Chelliah Y, Shan Y, Taylor CA, Yoo S-H, Partch C, et al. Crystal structure of the heterodimeric clock:*bmal1* transcriptional activator complex. *Science*. 2012;337(6091):189–94.
 58. Wang Z, Wu Y, Li L, Su X-D. Intermolecular recognition revealed by the complex structure of human clock-*bmal1* basic helix-loop-helix domains with E-box DNA. *Cell Research*. 2012;23(2):213–24.
 59. Tamaru T, Hattori M, Honda K, Nakahata Y, Sassone-Corsi P, van der Horst GTJ, et al. CRY drives cyclic CK2-mediated *bmal1* phosphorylation to control the mammalian circadian clock. *PLoS Biology*. 2015;13(11):1–25.
 60. Sahar S, Zocchi L, Kinoshita C, Borrelli E, Sassone-Corsi P. Regulation of *bmal1* protein stability and circadian function by GSK3 β -mediated phosphorylation. *Plos One*. 2010;5(1):e8561.
 61. Kwon I, Lee J, Chang SH, Jung NC, Lee BJ, Son GH, et al. BMAL1 shuttling

- controls transactivation and degradation of the clock/bmal1 heterodimer. *Molecular and Cellular Biology*. 2006;26(19):7318–30.
62. Lee J, Lee Y, Lee MJ, Park E, Kang SH, Chung CH, et al. Dual modification of bmal1 by sumo2/3 and ubiquitin promotes circadian activation of the clock/bmal1 complex. *Molecular and Cellular Biology*. 2008;28(19):6056–65.
63. Hirayama J, Sahar S, Grimaldi B, Tamaru T, Takamatsu K, Nakahata Y, et al. CLOCK-mediated acetylation of bmal1 controls circadian function. *Nature*. 2007;450(7172):1086–90.
64. Manwaring N, Jones MM, Wang JJ, Rohtchina E, Howard C, Mitchell P, et al. Population prevalence of the melas a3243g mutation. *Mitochondrion*. 2007;7(3):230–3.
65. Bender A, Krishnan KJ, Morris CM, Taylor GA, Reeve AK, Perry RH, et al. High levels of mitochondrial dna deletions in substantia nigra neurons in aging and parkinson disease. *Nature Genetics*. 2006;38(5):515–517.
66. Holt IJ, Harding AE, Morgan-Hughes JA. Deletions of muscle mitochondrial dna in patients with mitochondrial myopathies. *Nature*. 1988;331(6158):717–9.
67. Pavlakis SG, Phillips PC, DiMauro S, De Vivo DC, Rowland LP. Mitochondrial myopathy, encephalopathy, lactic acidosis, and strokelike episodes: a distinctive clinical syndrome. *Annals of Neurology*. 1984;16(4):481–8.
68. Suomalainen A, Isohanni P. Mitochondrial dna depletion syndromes - many genes, common mechanisms. *Neuromuscular Disorders*. 2010;20(7):429–37.
69. Patti M-E, Corvera S. The role of mitochondria in the pathogenesis of type 2 diabetes. *Endocrine Reviews*. 2010;31(3):364–95.
70. Shimamura A, Alter BP. Pathophysiology and management of inherited bone marrow failure syndromes. *Blood Reviews*. 2010;24(3):101–22.
71. Radelfahr F, Klopstock T. Mitochondrial diseases. *Nervenarzt*. 2019;90(2):121–30.
72. Wei MC, Zong W-X, Cheng EH-Y, Lindsten T, Panoutsakopoulou V, Ross AJ, et al. Proapoptotic bax and bak: a requisite gateway to mitochondrial dysfunction and

- death. *Science*. 2001;292(5517):727–30.
73. Wu C-C, Bratton SB. Regulation of the intrinsic apoptosis pathway by reactive oxygen species. *Antioxidants and Redox Signaling*. 2013;19(6):546–58.
74. Suski JM, Lebiezinska M, Bonora M, Pinton P, Duszynski J, Wieckowski MR. *Relation between mitochondrial membrane potential and ros formation*. New York: Humana Press; 2012.
75. Clerkin JS, Naughton R, Quiney C, Cotter TG. Mechanisms of ros modulated cell survival during carcinogenesis. *Cancer Letters*. 2008;266(1):30–6.
76. Tan Z, Luo X, Xiao L, Tang M, Bode AM, Dong Z, et al. The role of pgc1 α in cancer metabolism and its therapeutic implications. *Molecular Cancer Therapeutics*. 2016;15(5):774–82.
77. Matsuda S. Functions and characteristics of pink1 and parkin in cancer. *Frontiers in Bioscience*. 2015;20(3):491–501.
78. Kasahara A, Scorrano L. Mitochondria: from cell death executioners to regulators of cell differentiation. *Trends in Cell Biology*. 2014;24(12):761–70.
79. Gonzalez-Freire M, De Cabo R, Bernier M, Sollott SJ, Fabbri E, Navas P, et al. Reconsidering the role of mitochondria in aging. *Journals of Gerontology - Series A Biological Sciences and Medical Sciences*. 2015;70(11):1334–42.
80. Freya TG, Mannellab CA. The internal structure of mitochondria. *Trends in Biochemical Sciences*. 2000;25(7):319–24.
81. Fernie AR, Carrari F, Sweetlove LJ. Respiratory metabolism: glycolysis, the tea cycle and mitochondrial electron transport. *Current Opinion in Plant Biology*. 2004;7(3):254–61.
82. Schulz H. Beta oxidation of fatty acids. *Biochimica et Biophysica Acta (BBA) - Lipids and Lipid Metabolism*. 1991;1081(2):109–20.
83. Nsiah-Sefaa A, McKenzie M. Combined defects in oxidative phosphorylation and fatty acid oxidation in mitochondrial disease. *Bioscience Reports*. 2016;36(2):e00313–e00313.

84. Blacker TS, Duchen MR. Investigating mitochondrial redox state using nadh and nadph autofluorescence. *Free Radical Biology and Medicine*. 2016;100:53–65.
85. Starkov AA. “Mild” uncoupling of mitochondria. *Bioscience Reports*. 1997;17(3):273–9.
86. Brennan JP, Berry RG, Baghai M, Duchen MR, Shattock MJ. FCCP is cardioprotective at concentrations that cause mitochondrial oxidation without detectable depolarisation. *Cardiovascular Research*. 2006;72(2):322–30.
87. Amara CE, Shankland EG, Jubrias SA, Marcinek DJ, Kushmerick MJ, Conley KE. Mild mitochondrial uncoupling impacts cellular aging in human muscles in vivo. *Proceedings of the National Academy of Sciences*. 2007;104(3):1057–62.
88. Cadenas S. Mitochondrial uncoupling, ros generation and cardioprotection. *Biochimica et Biophysica Acta - Bioenergetics*. 2018;1859(9):940–50.
89. Ramsey KM, Yoshino J, Brace CS, Abrassart D, Kobayashi Y, Marcheva B, et al. Circadian clock feedback cycle through nampt-mediated nad⁺ biosynthesis. *Science*. 2009;324(5927):651–4.
90. Cela O, Scrima R, Paziienza V, Merla G, Benegiamo G, Augello B, et al. Clock genes-dependent acetylation of complex i sets rhythmic activity of mitochondrial oxphos. *Biochimica et Biophysica Acta - Molecular Cell Research*. 2016;1863(4):596–606.
91. Peek CB, Affinati AH, Ramsey KM, Kuo H, Yu W, Sena LA, et al. Circadian clock nad⁺ cycle drives mitochondrial oxidative metabolism in mice. *Science*. 2013;342(6158):1–17.
92. Schmitt K, Grimm A, Dallmann R, Oettinghaus B, Restelli LM, Witzig M, et al. Circadian control of drp1 activity regulates mitochondrial dynamics and bioenergetics. *Cell Metabolism*. 2018;27(3):657-666.e5.
93. Reddy AB, Karp NA, Maywood ES, Sage EA, Deery M, O’Neill JS, et al. Circadian orchestration of the hepatic proteome. *Current Biology*. 2006;16(11):1107–15.
94. Kohsaka A, Das P, Hashimoto I, Nakao T, Deguchi Y, Gouraud SS, et al. The

- circadian clock maintains cardiac function by regulating mitochondrial metabolism in mice. *Plos One*. 2014;9(11):e112811.
95. Chaix A, Zarrinpar A, Panda S. The circadian coordination of cell biology. *Journal of Cell Biology*. 2016;215(1):15–25.
 96. Gooley JJ. Circadian regulation of lipid metabolism. *Proceedings of the Nutrition Society*. 2016;75(04):440–50.
 97. Adamovich Y, Rousso-Noori L, Zwihaft Z, Neufeld-Cohen A, Golik M, Kraut-Cohen J, et al. Circadian clocks and feeding time regulate the oscillations and levels of hepatic triglycerides. *Cell Metabolism*. 2014;19(2):319–30.
 98. Poggiogalle E, Jamshed H, Peterson CM. Circadian regulation of glucose, lipid, and energy metabolism in humans. *Metabolism: Clinical and Experimental*. 2018;84:11–27.
 99. Liu C, Li S, Liu T, Borjigin J, Lin JD. Transcriptional coactivator pgc-1 α integrates the mammalian clock and energy metabolism. *Nature*. 2007;447(7143):477–81.
 100. Andrews JL, Zhang X, McCarthy JJ, McDearmon EL, Hornberger TA, Russell B, et al. CLOCK and bmal1 regulate myod and are necessary for maintenance of skeletal muscle phenotype and function. *Proceedings of the National Academy of Sciences*. 2010;107(44):19090–5.
 101. Peek CB, Ramsey KM, Levine DC, Marcheva B, Perelis M, Bass J. *Circadian regulation of cellular physiology*. Cambridge: Academic Press;2015.
 102. Gong C, Li C, Qi X, Song Z, Wu J, Hughes ME, et al. The daily rhythms of mitochondrial gene expression and oxidative stress regulation are altered by aging in the mouse liver. *Chronobiology International*. 2015;32(9):1254–63.
 103. Nogueiras R, Habegger KM, Chaudhary N, Finan B, Banks AS, Dietrich MO, et al. Sirtuin 1 and sirtuin 3: physiological modulators of metabolism. *Physiological Reviews*. 2012;92(3):1479–514.
 104. Nakahata Y, Kaluzova M, Grimaldi B, Sahar S, Hirayama J, Chen D, et al. The nad⁺-dependent deacetylase sirt1 modulates clock-mediated chromatin remodeling

- and circadian control. *Cell*. 2008;134(2):329–40.
105. Nakahata Y, Sahar S, Astarita G, Kaluzova M, Sassone-Corsi P. Circadian control of the nad⁺ salvage pathway by clock-sirt1. *Science*. 2009;324(5927):654–7.
 106. Asher G, Gatfield D, Stratmann M, Reinke H, Dibner C, Kreppel F, et al. SIRT1 regulates circadian clock gene expression through per2 deacetylation. *Cell*. 2008;134(2):317–28.
 107. Foteinou PT, Venkataraman A, Francey LJ, Anafi RC, Hogenesch JB, Doyle FJ. Computational and experimental insights into the circadian effects of sirt1. *Proceedings of the National Academy of Sciences*. 2018;115(45):11643–8.
 108. Wang RH, Zhao T, Cui K, Hu G, Chen Q, Chen W, et al. Negative reciprocal regulation between sirt1 and per2 modulates the circadian clock and aging. *Scientific Reports*. 2016;6:28633.
 109. Menzies KJ, Zhang H, Katsyuba E, Auwerx J. Protein acetylation in metabolism-metabolites and cofactors. *Nature Reviews Endocrinology*. 2016;12(1):43–60.
 110. Feldman JL, Dittenhafer-Reed KE, Denu JM. Sirtuin catalysis and regulation. *Journal of Biological Chemistry*. 2012;287(51):42419–27.
 111. Damiola F, Schibler U, Gene C-. A serum shock induces circadian gene expression in mammalian tissue culture cells. *Cell*. 1998;93(6):929–37.
 112. Cornelissen G. Cosinor-based rhythmometry. *Theoretical Biology and Medical Modelling*. 2014;11(1):1–24.
 113. Desquiret V, Loiseau D, Jacques C, Douay O, Malthiery Y, Ritz P, et al. Dinitrophenol-induced mitochondrial uncoupling in vivo triggers respiratory adaptation in hepg2 cells. *Biochimica et Biophysica Acta*. 2006;1757(1):21–30.
 114. Johnson L V, Walsh ML, Chen LB. Localization of mitochondria in living cells with rhodamine 123. *Proceedings of the National Academy of Sciences*. 1980;77(2):990–4.
 115. Whiteman M, Rose P, Jia LS, Nam SC, Gek ST, Halliwell B, et al. Hypochlorous acid-mediated mitochondrial dysfunction and apoptosis in human hepatoma hepg2

- and human fetal liver cells: role of mitochondrial permeability transition. *Free Radical Biology and Medicine*. 2005;38(12):1571–84.
116. Presley AD, Fuller KM, Arriaga EA. MitoTracker green labeling of mitochondrial proteins and their subsequent analysis by capillary electrophoresis with laser-induced fluorescence detection. *Journal of Chromatography B: Analytical Technologies in the Biomedical and Life Sciences*. 2003;793(1):141–50.
117. Wai T, Langer T. Mitochondrial dynamics and metabolic regulation. *Trends in Endocrinology and Metabolism*. 2016;27(2):105–17.
118. Otto F. *DAPI staining of fixed cells*. Cambridge: Academic Press;1990.
119. Sahar S, Masubuchi S, Eckel-Mahan K, Vollmer S, Galla L, Ceglia N, et al. Circadian control of fatty acid elongation by sirt1 protein-mediated deacetylation of acetyl-coenzyme a synthetase 1. *Journal of Biological Chemistry*. 2014;289(9):6091–7.
120. Ali I, Conrad RJ, Verdin E, Ott M. Lysine acetylation goes global: from epigenetics to metabolism and therapeutics. *Chemical Reviews*. 2018;118(3):1216–52.
121. Aguilar-Arnal L, Ranjit S, Stringari C, Orozco-Solis R, Gratton E, Sassone-Corsi P. Spatial dynamics of sirt1 and the subnuclear distribution of nadh species. *Proceedings of the National Academy of Sciences*. 2016;113(45):12715–20.
122. Anderson KA, Madsen AS, Olsen CA, Hirschey MD. Metabolic control by sirtuins and other enzymes that sense nad⁺, nadh, or their ratio. *Biochimica et Biophysica Acta - Bioenergetics*. 2017;1858(12):991–8.
123. Desquiret-Dumas V, Gueguen N, Leman G, Baron S, Nivet-Antoine V, Chupin S, et al. Resveratrol induces a mitochondrial complex i-dependent increase in nadh oxidation responsible for sirtuin activation in liver cells. *Journal of Biological Chemistry*. 2013;288(51):36662–75.
124. Cantó C, Gerhart-Hines Z, Feige JN, Lagouge M, Noriega L, Milne JC, et al. AMPK regulates energy expenditure by modulating nad⁺ metabolism and sirt1 activity. *Nature*. 2009;458(7241):1056–60.

125. Zheng X, Zhao X, Zhang Y, Tan H, Qiu B, Ma T, et al. RAE1 promotes bmal1 shuttling and regulates degradation and activity of clock: bmal1 heterodimer. *Cell Death and Disease*. 2019;10(2):62.
126. Ugalde C, Vogel R, Huijbens R, van der Heuvel B, Smeitink J, Nijtmans L. Human mitochondrial complex I assembles through the combination of evolutionary conserved modules: a framework to interpret complex I deficiencies. *Human Molecular Genetics*. 2004;13(20):2461–72.
127. Baracca A, Chiaradonna F, Sgarbi G, Solaini G, Alberghina L, Lenaz G. Mitochondrial complex I decrease is responsible for bioenergetic dysfunction in k-ras transformed cells. *Biochimica et Biophysica Acta - Bioenergetics*. 2010;1797(2):314–23.